Gondwana Research 148 (2025) 220–239

Contents lists available at ScienceDirect

Gondwana Research

journal homepage: www.elsevier.com/locate/gr

Core-refracted shear-wave anisotropy beneath the Korean Peninsula: insights into its tectonic evolution

Samuel Celis, Tae-Kyung Hong *, Junhyung Lee, Seongjun Park, Yanbing Liu, Byeongwoo Kim, Jeongin Lee, Dong Geon Kim

Department of Earth System Sciences, Yonsei University, Seoul, Republic of Korea

ARTICLE INFO

Keywords:
Seismic anisotropy
Shear-wave splitting
Collision
China blocks
Korean Peninsula

ABSTRACT

The tectonic history of the Korean Peninsula is marked by the Permo-Triassic collision between the North and South China blocks and the subsequently openings of the Yellow and East Seas during the Late Oligocene and Miocene. Despite well-constrained timing, the mechanisms behind these major tectonic episodes remain the subject of ongoing scientific debate. We studied seismic anisotropy from core-refracted shear-wave splitting to place constraints on lithospheric-scale and upper mantle structures and dynamics and provide insights into the tectonic evolution of the Korean Peninsula. We implemented the eigenvalue-based method to measure the splitting parameters and used the transverse energy minimization and cross-correlation techniques to validate our results. We found delay times ~ 1.5 s which is consistent with anisotropy residing in the asthenospheric and/or lithospheric mantle. Our results strongly suggest that the anisotropy signature of past tectonic events have been preserved and that the upper asthenosphere and lithosphere have undergone coherent deformation. Based on our model, we interpret that the Hongseong-Imjingang belt is part of the collision boundary, since we observed a lateral variation of the splitting parameters coinciding with it. We suggest two possible scenarios for the continuation of the collision suture beyond this belt: (1) one offshore with the boundary coinciding with the West Marginal Fault Zone, and (2) another one onshore along the southern limit of the Gyeonggi massif. Our observations support a fan-shaped opening mechanism for the East Sea and an eastward post-collisional extension for the Yellow Sea. Lastly, the measured splitting parameters beneath the western Gyeonggi and Yeongnam Precambrian massifs appear to be in good agreement with a possible fossil anisotropy.

1. Introduction

The current structure's complexity of the Korean Peninsula in eastern Asia is the result of different tectonic episodes that have been the focus of numerous investigations. Ultra-high metamorphic rocks along the Qinling-Dabie-Sulu belt in eastern China indicate the occurrence of a Permo-Triassic collision between the North China Block (Sino-Korean Craton) and the South China Block (Yangtze Craton) (Hu et al., 2022). However, the lack of occurrence of these rocks within and around the Korean Peninsula has made it difficult to trace the eastward continuation of the collision front. Consequently, many studies have investigated the mechanisms behind the collision and proposed different models to explain how and where it happened (e.g., Chang and Zhao, 2012; Chough et al., 2006; Hao et al., 2007; Kim et al., 2013; Kwon et al., 2009; Oh, 2006). After the collision and during the Oligocene and Miocene epochs, it has been proposed that both the Yellow and East Seas were opened. Both opening mechanisms have likewise been extensively studied and debated. For the Yellow Sea, E-W continental rifting and oceanic spreading have been proposed (e.g., Niu and Tang, 2016; Petrishchevsky, 2022), though the timing of its opening remains uncertain. In contrast, for the East Sea, fan-shaped (e.g., Otofuji et al., 1985; Otofuji and Matsuda, 1987) and pull-apart (e.g., Fournier et al., 1995; Lallemand and Jolivet, 1986) opening models have been suggested.

Seismic anisotropy is a frequently studied phenomenon that reflects directional dependence of seismic velocities. Within the upper mantle, it is produced by the lattice-preferred orientation of strong anisotropic minerals such as olivine or orthopyroxene (Long and Silver, 2009). Olivine minerals are the most abundant constituents of the Earth's upper mantle and it has been proven that they produce strong anisotropy when subjected to deformation processes (Karato et al., 2008). According to laboratory experiments, several olivine fabrics may develop depending on the stress field, water content, and temperature of the medium (Jung

* Corresponding author.
E-mail address: tkhong@yonsei.ac.kr (T.-K. Hong).

https://doi.org/10.1016/j.gr.2025.07.018
Received 23 January 2025; Received in revised form 9 June 2025; Accepted 23 July 2025
Available online 12 August 2025

et al., 2006; Karato et al., 2008; Kneller et al., 2005; Zhang and Karato, 1995). In stable cratonic lithospheres, such as beneath the Korean Peninsula, high temperatures and relatively low water content are typically expected. Consequently, the presence of A-type olivine fabric can be reasonably inferred.

A direct consequence of seismic anisotropy is the shear-wave splitting into two orthogonally polarized phases that travel along different planes at different speeds (Silver and Chan, 1991). This partitioning process can be quantified using two parameters: the fast polarization direction, ϕ, and the delay time until the arrival of the slow wave, δt.

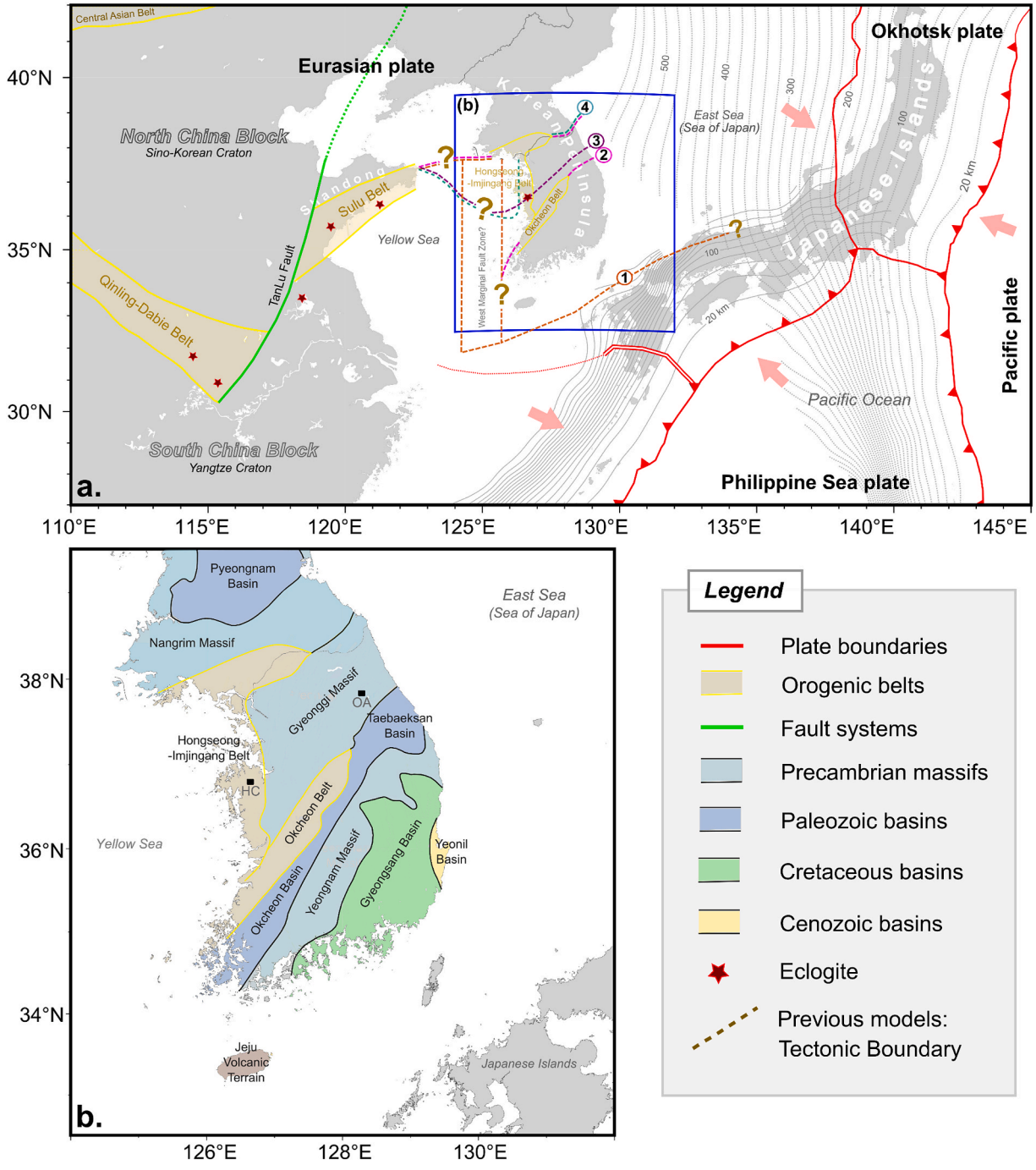

Fig. 1. Tectonic environment in eastern Asia: (a) Map showing the location of the Korean Peninsula in the easternmost part of the Eurasian plate, where the subductions of the Pacific and Philippine Sea plates occur beneath the Okhotsk and Eurasian plates. The Qinling-Dabie and Sulu belts, offset by the Tan-Lu fault, represent the collision boundary between the North and South China blocks in eastern China. The colored dashed lines with question marks denote previously-proposed collision boundaries in and around the Korean Peninsula: (1) along the West Marginal Fault Zone (Chang and Zhao, 2012; Hao et al., 2007; Hu et al., 2022; Kwon et al., 2009; Zhai et al., 2007), (2) along the South Korean Tectonic Line (Chough et al., 2006, 2000; Yin and Nie, 1993), (3) within the Gyeonggi massif (Choi et al., 2006; Oh, 2006; Oh et al., 2017), and (4) along the Hongseong-Imjingang belt (Kim et al., 2013; Kwon et al., 2009; Sajeev et al., 2010) (refer to the text for more details). The areas where eclogite phases have been found (Hu et al., 2022) are marked with a star. Light red arrows indicate the direction of absolute plate motions following the HS3-Nuvel1A model (Gripp and Gordon, 2002). The blue box corresponds to the region shown in (b). (b) Simplified geologic map of the Korean Peninsula (adapted from Kee et al., 2019). HS – Hongseong Complex, OA – Odesan Area (belt). (For interpretation of the references to color in this figure legend, the reader is referred to the web version of this article.)

These parameters are controlled by the anisotropic properties of the medium and the length of the ray paths through it (Savage, 1999; Silver and Chan, 1991). Core-refracted shear waves from teleseismic earthquakes are useful to investigate the anisotropy along the receiver side of the ray path from the core-mantle boundary to the surface. These waves derive from compressional waves travelling through the outer core, which is why their energy should be entirely along the radial direction (i.e., back-azimuth) unless there exists an anisotropic medium. In such case, the energy splits causing an elliptical rather than a linear particle motion polarization (Savage, 1999; Silver, 1996; Silver and Chan, 1991).

We propose to use core-transmitted phases such as *SKS* and *SKKS* to study the upper mantle anisotropy and place constraints on the tectonic evolution of the Korean Peninsula. Core-transmitted shear-wave anisotropy provides an opportunity to relate seismic observations to past and present tectonic anisotropy signatures. Due to upper mantle minerals' resistance to reorientation, they do not always directly represent the current stress field, thus the azimuthal anisotropy interpreted from *SK(K)S* splitting may reveal fossil fabrics in lithospheric-scale structures along with upper mantle dynamics (Silver, 1996; Silver and Chan, 1991).

2. Tectonic framework and unresolved issues

The Korean Peninsula, surrounded by the Yellow Sea and the East Sea (Sea of Japan), is situated in the easternmost part of the Eurasian plate where the Okhotsk, Pacific, and Philippine Sea plates converge (Fig. 1a). It constitutes a complex intraplate tectonic setting, evidenced by its structure and seismicity (e.g., Hong, 2010; Hong et al., 2023; Hong and Kang, 2009; Park et al., 2023), comprising the Yeongnam, Gyeonggi, and Nangrim Precambrian massifs, which are intersected by the Okcheon and Hongseong-Imjingang metamorphic belts. Within this setting, five major sedimentary basins have been identified: the Okcheon, Taebaeksan, and Pyeongnam Paleozoic basins, the Gyeongsang Cretaceous basin, and the Yeonil Cenozoic basin (Fig. 1b). It is hypothesized that the current morphology and geologic makeup of the Korean Peninsula are attributable to numerous tectonic events; the principal event is the collision between the North (Sino-Korean Craton) and South (Yangtze Craton) China blocks (Fig. 1a).

The Okcheon Phanerozoic belt, between the Gyeonggi and Yeongnam massifs, is a NE-trending fold-thrust belt whose sedimentation may have initiated during the Rodinia breakdown in the Neoproterozoic (Lee et al., 1998), although its cessation remains unclear. This metamorphic belt can be divided into two major zones based on tectonostratigraphic sequences: the southwestern Okcheon zone (basin) and the northeastern Taebaeksan zone (basin) (Chough et al., 2000; Jang et al., 2024; Oh, 2006) (Fig. 1). The former is composed of low- to intermediate-grade metamorphic rocks (Chough et al., 2000; Cluzel et al., 1991, 1990; Kim, 1996), while the latter presents non- or weakly metamorphosed sedimentary rocks (Chough et al., 2000). Although the Pyeongnam basin in northern Korean Peninsula is unquestionably part of the North China Block (Chang and Zhao, 2012), the tectonic provenance of the Okcheon and Taebaeksan basins remains a subject of ongoing debate (Fig. 1b). While some authors refer to the Okcheon belt as a tectonic boundary between the North and South China blocks, suggesting that the Okcheon basin accreted northeastward to the Taebaeksan basin along the dextral fault identified as the South Korean Tectonic Line (Chough et al., 2006, 2000; Yin and Nie, 1993), others believe that it represents a failed rift created along the suture zone between the Yangtze and Cathaysia cratons (within the South China Block) that was inverted to a contractional foreland basin (Jang et al., 2024; Oh, 2006). The absence of high- and ultra-high-grade metamorphic rocks along this belt supports the interpretation that it arose from compression caused by a distal collisional event (Oh, 2006; Oh et al., 2004b).

The recently defined Hongseong-Imjingang belt in western Korean Peninsula (Kee et al., 2019) is a narrow suture zone that separates the Nangrim massif from the Gyeonggi massif (Chough et al., 2000) and presents a grade of metamorphism that increases from north to south (Oh, 2006). It contains metasedimentary and plutonic rocks that were highly deformed during Permo-Triassic tectonic processes (Kwon et al., 2013; Park et al., 2017; Ree et al., 1996). Furthermore, high-pressure metamorphic rocks have been found in the Hongseong Complex with ages that match the eclogites from the Qinling-Dabie-Sulu belt (see Tables A1 and A2 in Hu et al., 2022), suggesting that the Hongseong area underwent high-pressure metamorphism equivalent to the collision episode that gave rise to the ultra-high pressure belt in eastern China (Fig. 1a).

During the Early to Middle Paleozoic, the North and South China blocks (Fig. 1a) separated from Gondwana and migrated northward while the Tethys Ocean was being consumed (Oh, 2006). These continental blocks collided starting from the eastern end (Korean Peninsula) in the Late Permian and propagating to the west (into the Shandong Peninsula) until the Late Triassic. The westward propagation occurred due to the clockwise rotation of about 67° of the South China Block relative to the North China Block (Chang and Zhao, 2012; Oh, 2006; Zhang, 1997). Numerous models have been proposed to explain this collision, which can be broadly classified into two major groups: models proposing offshore collision boundary near the west coast of the Korean Peninsula along the Western Marginal Fault Zone (also known as the East Marginal Fault of the Yellow Sea, Yellow Sea Transform Fault or Wrench Fault System within the West Sea), and models proposing an inland collision boundary within the Korean Peninsula.

Offshore tectonic boundary. – Several authors support models that place the tectonic boundary along or near the west coast of the Korean Peninsula (Fig. 1a). Hao et al. (2007) interpret the Western Marginal Fault Zone as a dextral strike-slip system and consider it as the counterpart of the Tan-Lu sinistral fault in eastern China (Fig. 1a). In addition, Zhai et al. (2007) and Kwon et al. (2009) propose crustal-detachment models where the collision suture is located along the west margin of the Korean Peninsula coinciding with the Hongseong-Imjingang belt (Kee et al., 2019). They believe that the Hongseong Complex, where eclogite minerals have been reported (Kim et al., 2006; Oh et al., 2017, 2005, 2004a; Park et al., 2014), is directly related to the collision front (exhumation and/or crustal detachment). Similarly, Chang and Zhao (2012) and Hu et al. (2022) suggest that the Yellow Sea Transform Fault is the eastern boundary of the South China Block, arguing that the collision occurred in several stages including contact and subduction, relative clockwise rotation of the South China Block, collision and suturing (orogenesis), and post-collisional extension. The clockwise rotation may have produced intense deformation in the Korean Peninsula along the Yellow Sea Transform Fault.

Inland tectonic boundary. – On the other hand, some authors suggest that the collision boundary is located within the Korean Peninsula. Chough et al. (2006, 2000), Li (1994), and Yin and Nie (1993) argue that the Okcheon basin and Gyeonggi massif accreted northeastward to the Tabaeksan basin and Yeongnam massif along the South Korean Tectonic Line, which they interpret as the counterpart of the left-slip Tan-Lu fault. They believe that, following an indentation model, the Gyeonggi massif (South China Block) began to collide with the Nangrim massif (North China Block) at the Imjingang belt, causing the separation of the Yeongnam massif from the rest of the North China Block (Fig. 1a). In contrast, Choi et al. (2006), Oh (2006), Oh et al. (2017), and Lee et al. (2019) suggest that the Qinling-Dabie-Sulu belt in China extends to the Hongseong-Odesan belt in Korea and that the Okcheon belt should be correlated to the Nanhua rift between the Yangtze and Cathaysia cratons within the South China Block. These conclusions are drawn from the ages of high-pressure metamorphic rocks in the Hongseong-Odesan belt (297–255 Ma, when the collision happened) and from the fact that both the Okcheon and Imijingang belts are characterized by intermediate-P/T metamorphism indicative of distal collisional settings. The Hongseong-Odesan belt separates the Gyeonggi massif in two parts, which means that the authors believe that the northern and southern parts of the

Gyeonggi massif should be correlated to the North and South China blocks, respectively. Lastly, Kim et al. (2013) and Sajeev et al. (2010) propose tectonic models with a collision boundary similar to the one proposed by Kwon et al. (2009) along the Hongseong-Imjingang belt, with the difference that they suggest that the boundary continues inland along the limit area between the Nangrim and Gyeonggi massifs (Fig. 1a). According to them, both the Gyeonggi and Yeongnam massifs should be correlated with the South China Block.

Right after the collision, in the Early Jurassic (ca. 200 Ma), the northwestward subduction of the paleo-Pacific plate (often referred to as the Izanagi plate) under the Asian continent initiated along the southern margin of the Korean Peninsula (Chough et al., 2000; Kim et al., 2024). Based on the distribution of Jurassic granitoids throughout the peninsula, some authors suggest that the paleo-Pacific plate was initially subducted (ca. 200–190 Ma) at a high angle, forming NS- or NE-trending sedimentary basins, and then the subduction angle changed (ca. 182–164 Ma) from steep to shallow, producing shear zones in the crust such as the Honam shear zone (Cheong and Jo, 2020; Kawaguchi et al., 2023; Kee et al., 2010; Kim et al., 2011, 2021; S. W. Kim et al., 2015). It has been suggested that the Cretaceous Gyeongsang basin, the largest sedimentary basin in Korea, was formed in response to the NNW-directed subduction of the paleo-Pacific slab, with its eastward expansion attributed to slab rollback (e.g., Cheon et al., 2020; Chough et al., 2000; among others). Some authors argue that it is a forearc basin, a determination supported by the correlations of its sediments and volcanogenic components with the Jurassic accretionary complex in southwestern Japan (Lee et al., 2023; Lee and Kim, 2005; Lee and Lee, 2000). Conversely, some others explain that it was formed as a back-arc basin due to the extension caused by strike-slip movements that were induced by the subduction of the paleo-Pacific plate (Cheon et al., 2020; Cheong and Jo, 2017; Chough and Sohn, 2010; Kim et al., 2016).

The Yellow Sea, a Cenozoic continent-rifted basin (Fig. 1), allegedly began spreading prior to the opening of the East Sea (Sea of Japan) (ca. 27 Ma), before being interrupted by the northwestward subduction of the Philippine Sea plate in the Mid-Miocene (ca. 16 Ma) (Niu and Tang, 2016; Petrishchevsky, 2022). However, the exact timing of the Yellow Sea opening remains unclear. This post-collisional extension has been proposed by different authors (e.g. Kimura et al., 1990; Niu and Tang, 2016; Petrishchevsky, 2022) and they suggest that it was the result of mantle upwelling and decompression melting.

The Cenozoic tectonic regime in the eastern margin of the Korean Peninsula was characterized by the opening of the East Sea (Sea of Japan) (Fig. 1), resulting from a paleo rifting event that took place during the Oligocene-Miocene (ca. 23–15 Ma) (Choi et al., 2012; Hong et al., 2024, 2020; Jolivet et al., 1994; Kano et al., 2002; Kim et al., 2007; Son et al., 2015). Several kinematic models have been proposed to explain the opening mechanism of the East Sea. The most accepted one is the fan-shape (or bar-door) model wherein the SW Japanese Arc rotated clockwise away from the Korean Peninsula in response to back-arc rifting and spreading of the continental lithosphere (e.g., Otofuji et al., 1985; Otofuji and Matsuda, 1987, 1983). Following this model, some authors propose a counterclockwise rotation of NE Japan, leading to a double-sided door opening model (Otofuji et al., 1994; Vaes et al., 2019; Yang et al., 2022). Alternatively, a pull-apart mechanism between two strike-slip fault systems constitutes another model that has been proposed to explain the opening mode of the East Sea (Sea of Japan) (e.g., Fournier et al., 1995; Kimura and Tamaki, 1986; Lallemand and Jolivet, 1986), but it does not agree with paleomagnetic evidence (Otofuji et al., 1985; Otofuji and Matsuda, 1983).

In southwestern Korean Peninsula, the Jeju Island (also known as the Jeju Volcanic Terrain; Fig. 1b) constitutes a Cenozoic volcanic field that was formed in an intraplate setting whose volcanism started in the Early Pleistocene (Brenna et al., 2015; Lee et al., 2024; Sohn and Park, 2004; Song et al., 2018). This region has experienced extensional stresses due to the increased rollback of the Philippine Sea plate (Pacanovsky et al., 1999), producing trenchward mantle flow and probably localized mantle upwelling. Therefore, it is believed that the volcanic activity in the Jeju Island is driven by the stress field caused by the subduction of the Philippine Sea plate (Brenna et al., 2015).

3. Data and method

3.1. Data collection and preprocessing

We collected core-transmitted *S* waveforms from 245 earthquakes occurring between 2010 and 2024, with focal depths down to 600 km (event information is available in Table S1), recorded at 144 seismic stations, including 106 permanent (Korea Meteorological Administration, KMA; Korea Institute of Geoscience and Mineral Resources, KIGAM; and Japan Meteorological Agency, JMA) and 38 temporary (Yonsei University and Pusan National University) stations installed in central and southern Korean Peninsula (Fig. 2). The interstation distances range from 4 to 775 km, with a minimum average spacing of 23.3 km, which provides sufficient resolution to detect small-scale variations in anisotropy since the *SK(K)S* Fresnel zone size at surface is ~ 10–30 km (Alsina and Sneider, 1995). Sensor orientation angles of seismic stations were corrected according to Park and Hong (2024). By limiting the analysis to high-magnitude earthquakes ($M \geq 5.8$) occurring at epicentral distances between 85° and 140°, we aimed to select high signal-to-noise ratio *SKS* and *SKKS* waveforms that reach the surface stations with near-vertical incidence angles and without distortions from other teleseismic phases, such as direct or diffracted *S* waves. Data were filtered using a zero-phase Butterworth bandpass filter between 0.04 and 0.125 Hz. We employed automated selection criteria based on theoretical arrival times to identify and visually inspect waveforms. Only those exhibiting well-defined *SKS* and/or *SKKS* phases were retained for further analysis.

3.2. Method

We used the covariance method proposed by Silver and Chan (1991) to estimate the shear-wave splitting parameters (ϕ, δt). This method assumes the existence of a single layer of transverse anisotropy with a horizontal axis of symmetry below the station and is based on the minimization of the smallest eigenvalue (λ_2^{min}). A detailed example is shown in Fig. 3.

At first, we automatically select and visually check a time window no longer than 42 s (depending on the signal-to-noise ratio) from the north–south and east–west components, including the *SKS* or *SKKS* phases at the end (Fig. 3a). Then, we conduct a grid search wherein both components are rotated from −90° to 90° in 1° intervals and, for each rotation, one component is time-shifted relative to the other from 0 to 4 s in 0.05 s intervals. For each pair of test values, we calculate the covariance matrix and its eigenvalues to finally select the combination associated with λ_2^{min} (Fig. 3b), which corresponds to the most nearly singular covariance matrix and, therefore, to the best solution (Silver and Chan, 1991).

We estimate the uncertainty levels using an inverse *F* test following Silver and Chan (1991) (Fig. 3b). This test is based on the *F* probability distribution and assumes that λ_2^{min} follows a χ^2 distribution, which is a good estimation for a Gaussian white noise process. This procedure allows us to identify reliable non-null and null measurements. In general, measurements are considered null when the particle motion is originally parallel to either the fast or slow direction. In these cases, no energy is present on the transverse component, and the horizontal particle motion is linear, which indicates the absence of splitting beneath the station (Long and Silver, 2009; Silver and Chan, 1991; Wüstefeld and Bokelmann, 2007). We consider observations to be poor when energy is present on the transverse component, but the splitting parameters cannot be well constrained. Those measurements that present a closed 95 % confidence region of λ_2^{min} are used to conduct a two-step anisotropy

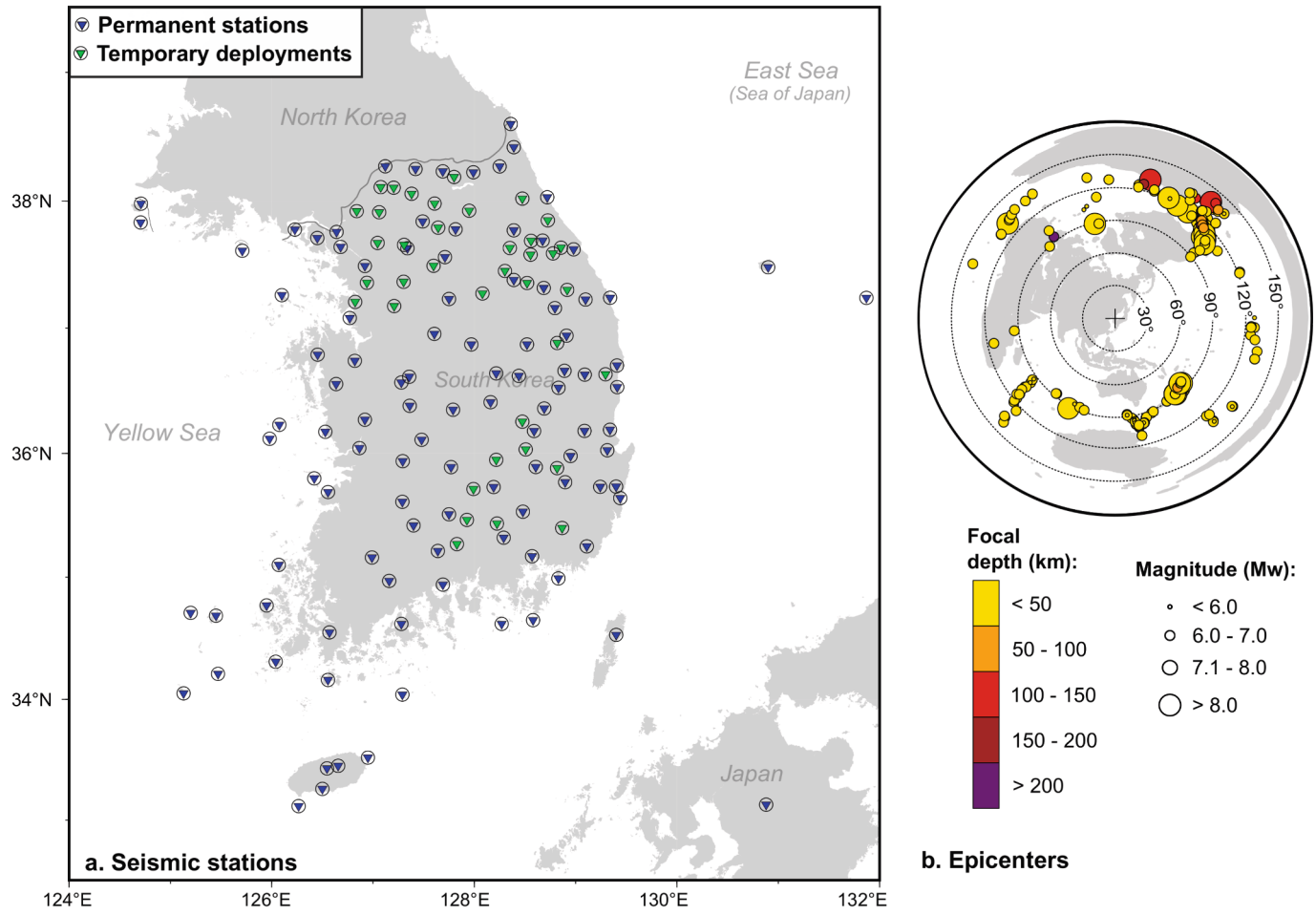

Fig. 2. (a) Broadband seismic permanent (106) and temporary (38) stations and (b) earthquakes (245) used to estimate core-refracted shear-wave splitting parameters to investigate seismic anisotropy beneath the central and southern Korean Peninsula.

correction that aims to verify that the splitting parameters describe the anisotropy below the station. At first, we time-shift the slow wave according to δt and visually verify that both fast and slow waves are into phase after the correction (Fig. 3c). Then, we calculate the corrected radial and transverse components from the corrected fast and slow waves and verify that the *SKS* or *SKKS* energy on the transverse is removed and returned to the radial component, which also implies that the corrected particle motion has been successfully linearized (Fig. 3d). Those measurements that are thoroughly verified are considered reliable and included in the next step of the process.

Finally, to corroborate our individual measurements, we estimate the splitting parameters using the maximum cross-correlation method (Bowman and Ando, 1987; Shih et al., 1989) and the transverse energy minimization (Silver and Chan, 1991). The estimated parameters using the three methods agreed in most cases (as shown in Fig. 3b). In cases where the parameters showed slight differences, we prioritized those that more effectively removed the anisotropy (i.e., those that better linearized the radial-transverse and fast-slow particle motions). To further illustrate the method, Fig. 4 presents examples of five reliable non-null observations and two reliable null observations.

We implemented the misfit surface stacking method proposed by Wolfe and Silver (1998), which enables us to reinforce the anisotropy patterns observed from single splitting observations, specifically in cases of single-layer anisotropy with horizontal axes of symmetry and/or unimodal splitting parameter distributions. This method consists of summing the normalized contour levels for all individual measurements and calculating again the minimum value of the resulting surface and its 95 % confidence interval. It allows to reduce the 95 % confidence region and the noise effects on the individual measurements. Fig. 5 shows an example of the misfit surface stacking method applied at station GEJB.

4. Results

Reliable core-refracted shear-wave splitting parameters are shown in Fig. 6 along with the epicenters and back-azimuths of all useful earthquakes that we used to analyze *SKS* and/or *SKKS* waveforms recorded at stations mapped in Fig. 2. We were able to find good azimuthal coverage of the events, even though most of them occurred in northeastern Pacific Ocean (Figs. 6d and 6e). This back-azimuthal distribution of the data enables the inspection of variations or consistency in splitting parameters. In the end, we detected 1093 useful source-to-receiver pairs and obtained 583 non-null and 510 null measurements (detailed lists of all non-null and null splitting results can be found in Tables S2 and S3, respectively).

We found normally distributed delay times with a mean value of 1.58 s and a standard deviation of 0.47 s, ranging from 0.60 to 2.95 s (see inset in Fig. 6a). These values are consistent with an anisotropy layer confined to the upper mantle (lithosphere and asthenosphere), since it may produce anisotropy strengths up to 5 % (from 0 to 3.0 s) whereas the crust (e.g., Barruol and Mainprice, 1993; Crampin, 1994; Silver, 1996), transition zone (e.g., Fouch and Fischer, 1996) and lower mantle (e.g., Vinnik et al., 1995) are each thought to contribute less than 2 % (less than 0.7 s) to anisotropy observations at surface (Savage, 1999).

From the individual non-null estimates shown in Fig. 6a, we identify four main regions based on fast directions (Fig. 6c) and tectonic features, since delay times are generally consistent across the study area. The first

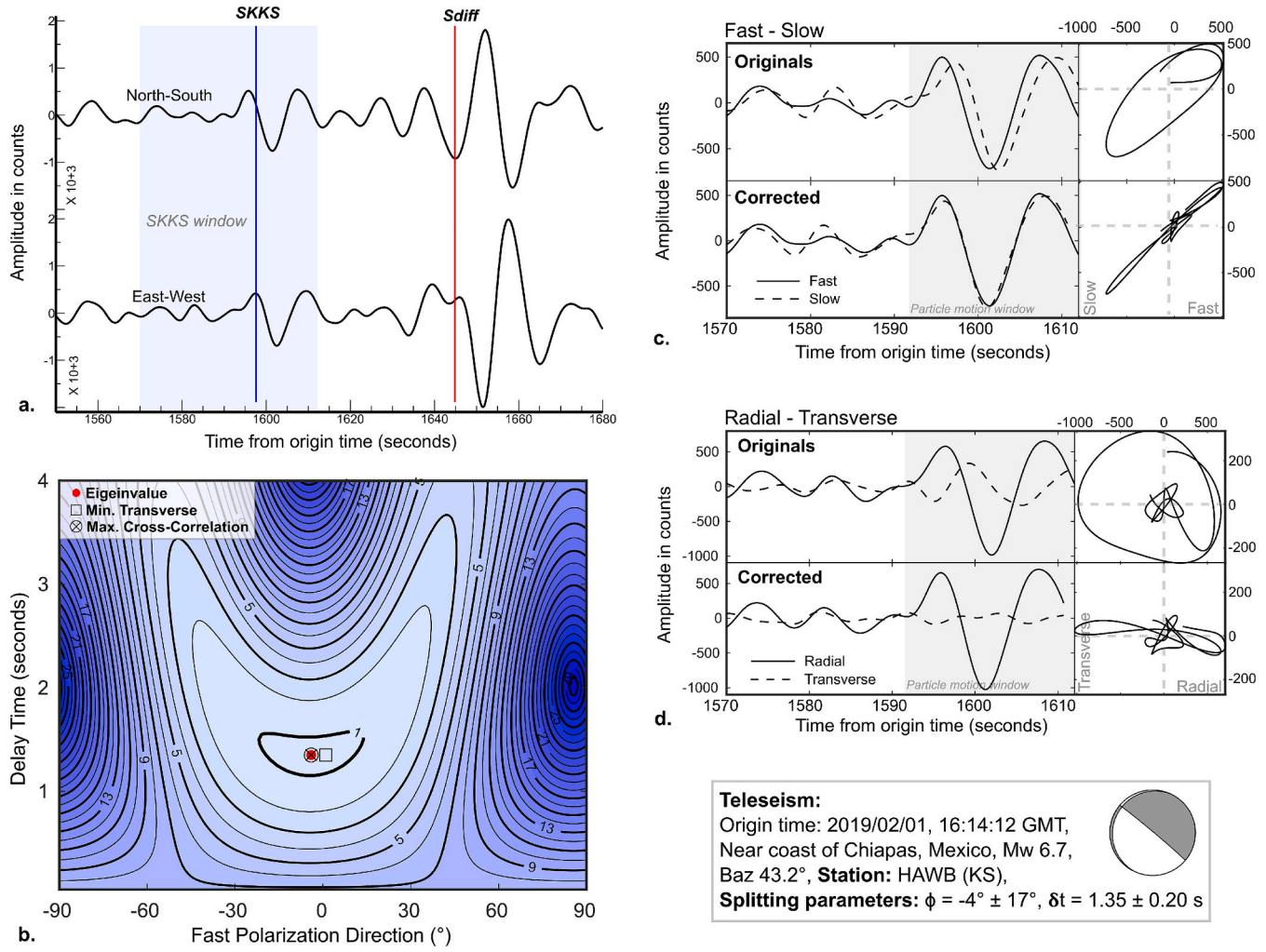

Fig. 3. High-quality shear-wave splitting measurement. (a) Original (filtered) horizontal components recorded at station HAWB (KS) showing the *SKKS* and the diffracted *S* phases from the M_w 6.7 earthquake that occurred in southern Mexico on February 1, 2019 (details and focal mechanism are provided in the white box). The blue-shaded area denotes the *SKKS* window. (b) Contour map showing the λ_2^{min} values from the grid search. The red dot indicates the best solution pair of splitting parameters ($\phi = -4^{\circ} \pm 17^{\circ}$, $\delta t = 1.35 \pm 0.20$ s). Contour numbers represent standard deviations. The splitting parameters estimated using the minimum transverse energy (box) and the maximum cross-correlation (crossed circle) methods are shown and used for validation. (c) Fast and slow waveforms and particle motions (plotted using the waveforms within the gray-shaded area) before (top) and after (bottom) removing the anisotropy. It can be seen that the correction brought the fast and slow waves into phase. (d) Original (top) and corrected (bottom) radial and transverse components, including their particle motion. (For interpretation of the references to color in this figure legend, the reader is referred to the web version of this article.)

region coincides with the Yeongnam massif in the central southern part of the Korean Peninsula, and it shows an overall fast polarization oriented in the NW-SE direction. Moving westward and southwestward, fast axes rotate and become oriented closer to the E-W direction, comprising the second region that we identify. This region also includes observations from stations on Jeju Island. On the other hand, N-S and NE-SW fast directions observed from the southeastern Korean Peninsula, extending to Japan's Tsushima Island and further to Ulleung and Dokdo islands in the East Sea (Sea of Japan), constitute the third region. In this region we also include NNW-SSE oriented fast axes observed at a single station inland in Japan, despite the fact they show a different orientation. Lastly, we identify a fourth region that approximately encompasses the Hongseong-Imjingang belt, the Gyeonggi massif, and the Taebaeksan basin (from west to east) in the northern part of the study area. This region exhibits a predominant NE-SW oriented fast direction that coincides with the western part of the Gyeonggi massif. Offshore in the west, we observe a slight different trend of fast axes oriented approximately N-S that appears to terminate along the Hongseong-Imjingang belt. Farther inland to the east, in the area that corresponds to the eastern Gyeonggi massif and to the Taebaeksan basin, we identify another trend characterized by a slight clockwise rotation of the fast axes, which differs from observations made at the Ulleung island in the East Sea (Sea of Japan).

Null observations (Fig. 6b) refine the fast directions associated with non-null measurements and, therefore, the identification of the four regions. In general, we observe that the back-azimuth of waves associated with nulls are either parallel or perpendicular to the overall fast directions of the non-null measurements shown in Fig. 6a. Moreover, stations located in the southeastern and northwestern parts of the study area exhibit only a few nulls, while the others exhibit a large number. This conforms to our expectations because the back-azimuth distribution of the earthquakes (mainly from the NE) is well-suited for measuring the approximately N-S fast polarization directions observed in the southeastern and northwestern parts of the region. However, in other regions, most earthquake back-azimuths are either parallel or perpendicular to the non-null fast directions, leading to null measurements.

In Fig. 7 we show back-azimuthal plots, rose diagrams, and stacked contour levels to illustrate individual and stacked splitting results computed at three stations. Rose diagrams and back-azimuthal plots

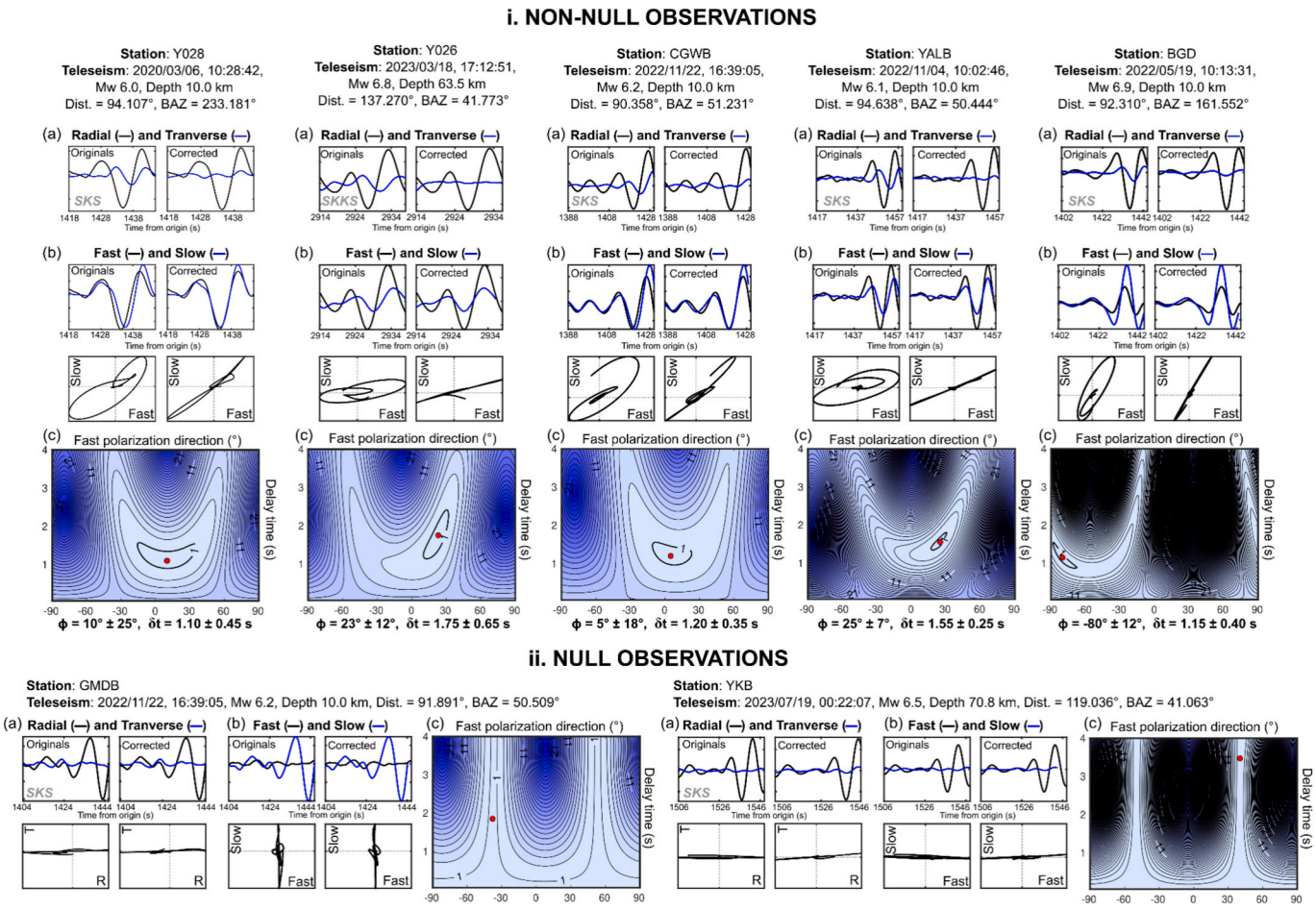

Fig. 4. Examples of reliable (i) non-null and (ii) null observations. (a) Original and corrected radial and transverse components (particle motion plots are included in case of nulls), (b) original and corrected fast and slow components and their particle motion before and after the correction, (c) misfit contour surface showing the optimal splitting parameters (red dot). (For interpretation of the references to color in this figure legend, the reader is referred to the web version of this article.)

show unimodal behavior of the observed splitting parameters for most stations. This may signal that the anisotropy beneath the Korean Peninsula is simple and resides in a single layer, likely within the upper 200 km of the mantle (Savage, 1999; Silver, 1996). In case of multiple layers of anisotropy (i.e., vertically stratified anisotropic medium), a back-azimuthal dependence of apparent splitting parameters should occur, and they should exhibit systematic variations as a function of the incoming polarization with $\pi/2$ or π periodicity (Silver and Savage, 1994). Our estimates do not support these complex structures, although some stations exhibit lateral variations in splitting parameters, as discussed below. Additionally, stacked contour plots from Fig. 7 show small and well-constrained 95 % confidence regions, indicating that stacked anisotropy parameters are well-constrained and that uncertainty from individual estimates has been successfully reduced (Wolfe and Silver, 1998).

Along the Hongseong-Imjingang belt and approximately along the limit between the Gyeonggi and Yeongnam massifs (Fig. 1), splitting parameters are more scattered (Fig. 6) but show no clear evidence of multiple anisotropic layers. Instead, the observed variations suggest that anisotropy in the uppermost part of the upper mantle is heterogeneous (above 250 km depth) (e.g., Alsina and Sneider, 1995; Plomerová et al., 1996; Savage, 1999), with fast axes oriented NE-SW in the northern region and NW-SE in the southern region. To investigate consistency and possible lateral changes of anisotropy directions across this area, we project the splitting parameters to different depths. We choose depths of 50, 100, 150, 200, and 250 km and project the parameters to the corresponding piercing-point locations (Fig. 8). With greater depth, the spatial distribution of the *SK(K)S* ray piercing points expands outwards from the stations, leading to their eventual superimposition. As shown in Fig. 8, there exists a high consistency or similarity between the splitting parameters down to a depth of 200 km. At 250 km, the transition zone between the two main splitting parameter patterns becomes diffuse, suggesting that the layer of anisotropy is located above this depth. It is noteworthy that a similar case of lateral variation in splitting parameters may occur in the southeastern part of the Korean Peninsula; however, the contrast is less distinct.

We compare the splitting parameters from two different events with opposite back-azimuths recorded at stations KIP and SEO3, both situated along the Hongseong-Imjingang belt. We compute their Fresnel zones (i.e., elliptical regions around the ray path where the finite-frequency wave interference affects signal propagation) down to 200 km depth to visualize the common paths between the phases as the Fresnel zone radius increases with depth (Fig. 9). At station KIP, we compare a *SKS* phase with a back-azimuth of 51°, an incidence angle of 7.7° and a period of 9 s with another *SKS* with a back-azimuth of 233°, an incidence angle of 9.5° and a period of 11 s, while at station SEO3, we compare a *SKKS* phase with a back-azimuth of 45°, an incidence angle of 11.8° and a period of 12.6 s with another *SKKS* with a back-azimuth of 231°, an incidence angle of 11.9° and a period of 13 s. As can be seen in Fig. 9, the observed splitting parameters for both groups of back-azimuths are different. Those computed with phases with back-azimuths around 50° show a NE-SW fast polarization direction, while those computed with phases with back-azimuths around 230° show an NNW-SSE fast polarization direction. This lateral variation is attributed to the fact that core-

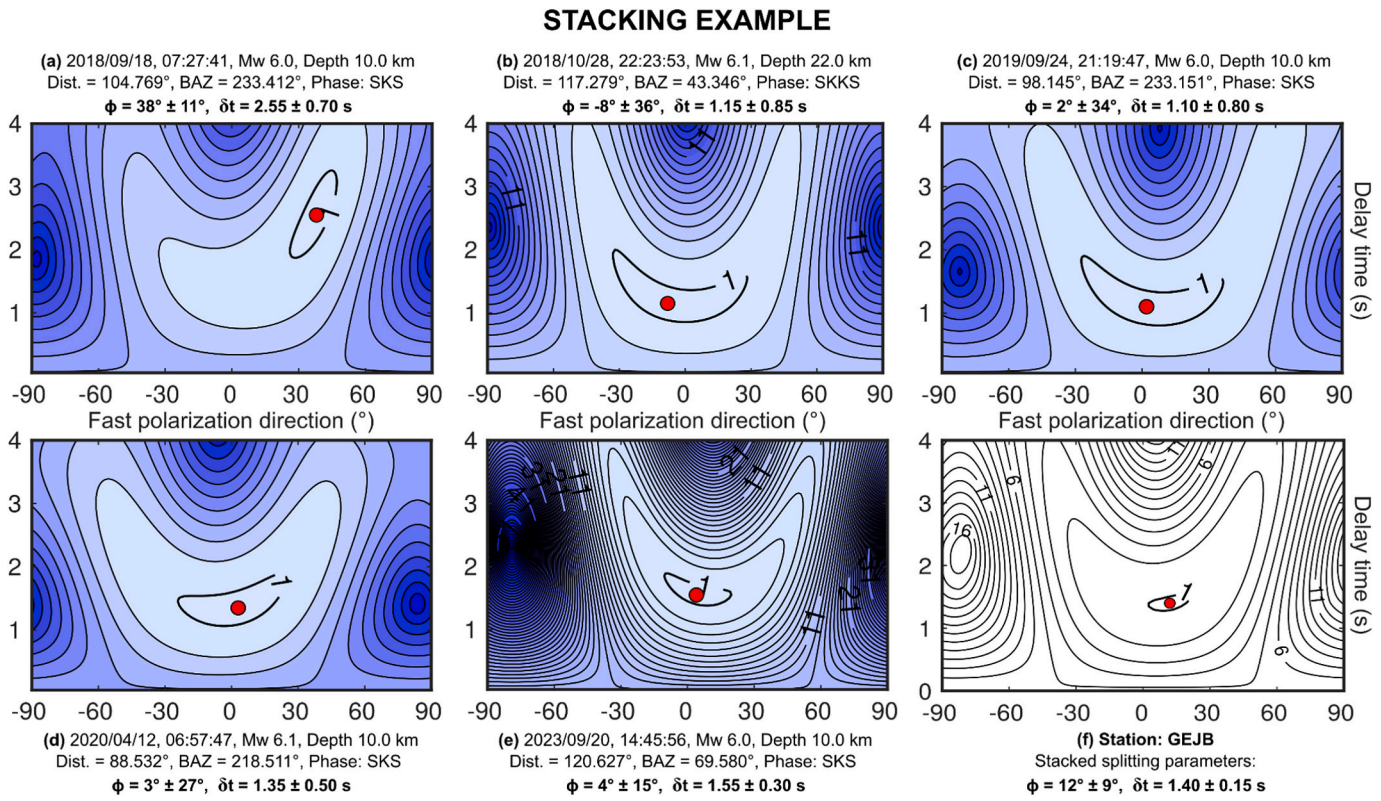

Fig. 5. Example of the misfit surface stacking method (Wolfe and Silver, 1998) applied at station GEJB. (a, b, c, d, e) Misfit maps of five individual measurements were used to obtain (f) the stacked error surface. Red dots correspond to the best solution (λ_2^{min}) of individual and stacked parameters. (For interpretation of the references to color in this figure legend, the reader is referred to the web version of this article.)

refracted waves sample different anisotropic regions in the upper mantle, depending on their back-azimuth.

Station-stacked splitting estimates using the method of Wolfe and Silver (1998) are shown in Fig. 10 and listed in Table S4. We computed 118 well-constrained, 13 poorly constrained, and 13 unconstrained stacked parameters. Stacked measurements with large uncertainty values (i.e., $\sigma_\phi \geq 35^\circ$ and $\sigma_{\delta t} \geq 0.50s$) are considered as poorly constrained. These, along with unconstrained measurements from single observations at individual stations, are shown as red bars in Fig. 10. Rather than visualizing each individual measurement, the stacking process provides a stable, representative estimate of the dominant splitting direction in cases where the individual observations are not too scattered. It also allows us to estimate the depth and thickness of the anisotropy source beneath each station. The stacked results are on average $\phi_{mean} = -5^\circ$ and $\delta t_{mean} = 1.38s$ and exhibit similar patterns to the individual estimates (Fig. 10a), except for the NE-SW fast axes observed at some stations in the southeasternmost part of the region and for the lateral variation of anisotropy illustrated in Fig. 8, which is clearer from the individual results.

5. Depth constraint and validation test

To investigate the depth and source of the anisotropic layer, we use the expression proposed by Helffrich (1995) and Silver and Chan (1988) and assume a peridotite mantle composition (i.e., 70 % olivine and 30 % orthopyroxene). This expression allows us to constrain the depth of the anisotropic source based on the station-averaged delay time, the shear-wave velocity for the upper mantle, and the anisotropy percentage (details are provided in the supplementary material). According to our results (see Table S4), the depth of the anisotropic layer bottom is approximately 180 km and the mean thickness is about 148 km, since the depth of the Moho discontinuity for the study region is around 32 km (Lee et al., 2022) (see Fig. S1 in the supplementary material). These values along with the strong correlation between the fast axis orientations and the tectonic features suggest a shallow anisotropy and are consistent with the depth limit of the anisotropic layer interpreted for the lithospheric mantle in stable continental regions far from subduction systems (Savage, 1999; Silver, 1996; Silver and Chan, 1991).

We conduct a validation test using the particle motion perturbation method of Fischer et al. (2000) to simulate synthetic waveforms with forward modeling that replicate the observed seismograms, which is essential for model verification. A representative example is illustrated in Fig. 11. For each case, we first define a simple wavelet with a linear horizontal particle motion and a polarization along the back-azimuth of the observed phase (Fig. 11a). This aims to simulate a receiver-side *SK(K)S* propagating through an isotropic and homogeneous medium, with its energy entirely along the radial direction. The target period of pulse is determined using the Fourier transform of the observed seismograms.

After creating the synthetic pulse, we define an anisotropic layer between a lower half-space and an overlying 32-km thick isotropic crust. The layer thickness is estimated from the station-stacked delay times, as mentioned above (see supplementary materials for more details). We use elastic coefficients and their pressure and temperature derivatives from the existing literature (Abramson et al., 1997; Anderson and Isaak, 1995; Frisillo and Barsch, 1972). These values allow us to estimate elastic constants at depth assuming an orthorhombic symmetry where the olivine *a*, *b* and *c* axes align with the orthopyroxene *c*, *a* and *b* axes, respectively, which constitutes the ideal orientation in the upper mantle (Christensen, 1984; Mainprice and Silver, 1993). The elastic constants are estimated for a depth value determined by the midpoint of the anisotropic layer and the olivine *a*-axis orientation is defined from the station-stacked fast polarization directions (see Table S2). After determining the stiffnesses and orientation at depth, we use the Christoffel matrix (Babuska and Cara, 1991) to find phase velocities and the fast

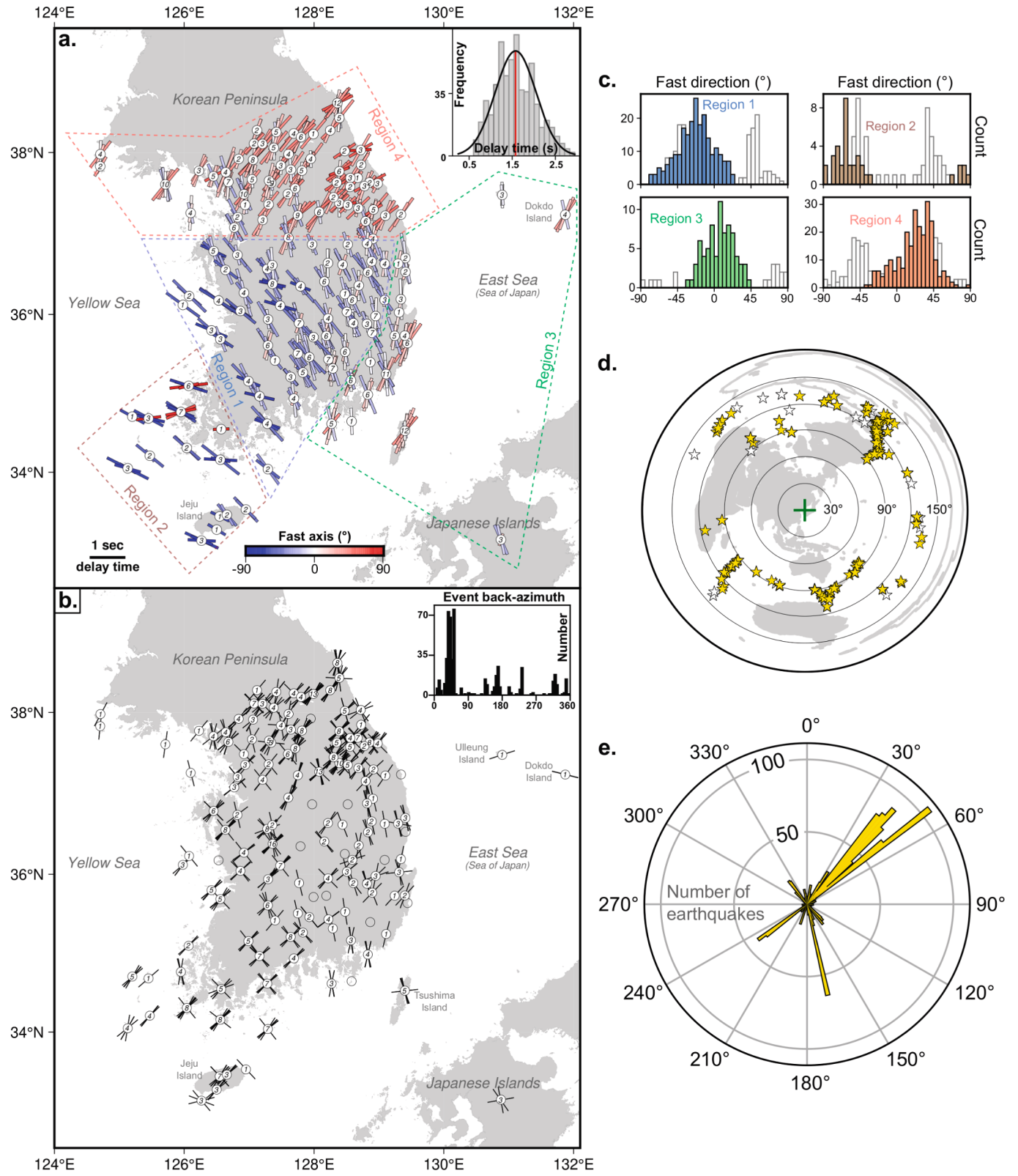

Fig. 6. (a) Map showing 583 individual *SKS* and *SKKS* reliable non-null measurements. Bars representing shear-wave splitting parameters are color coded according to legend. Their length is defined by δt and their orientation is given by ϕ. Dashed lines enclose regions of different fast directions, as defined herein. Top right inset: histogram of observed delay times, averaging 1.58 s (red solid line) with a standard deviation of 0.47 s. (b) Map showing back-azimuth of the 510 waves with null observations. Top right inset: histogram detailing the back-azimuth distribution of these null-associated waves. Numbers within the circles representing seismic stations in (a) and (b) correspond to the number of non-null and null observations in each case. (c) Histograms showing the fast axes of each region that we identify. White bars in the background indicate fast directions associated with nulls. (d) Epicenters of the useful earthquakes: yellow and white colors indicate resulting non-null and null measurements, respectively. (d) Back-azimuth of the earthquakes. (For interpretation of the references to color in this figure legend, the reader is referred to the web version of this article.)

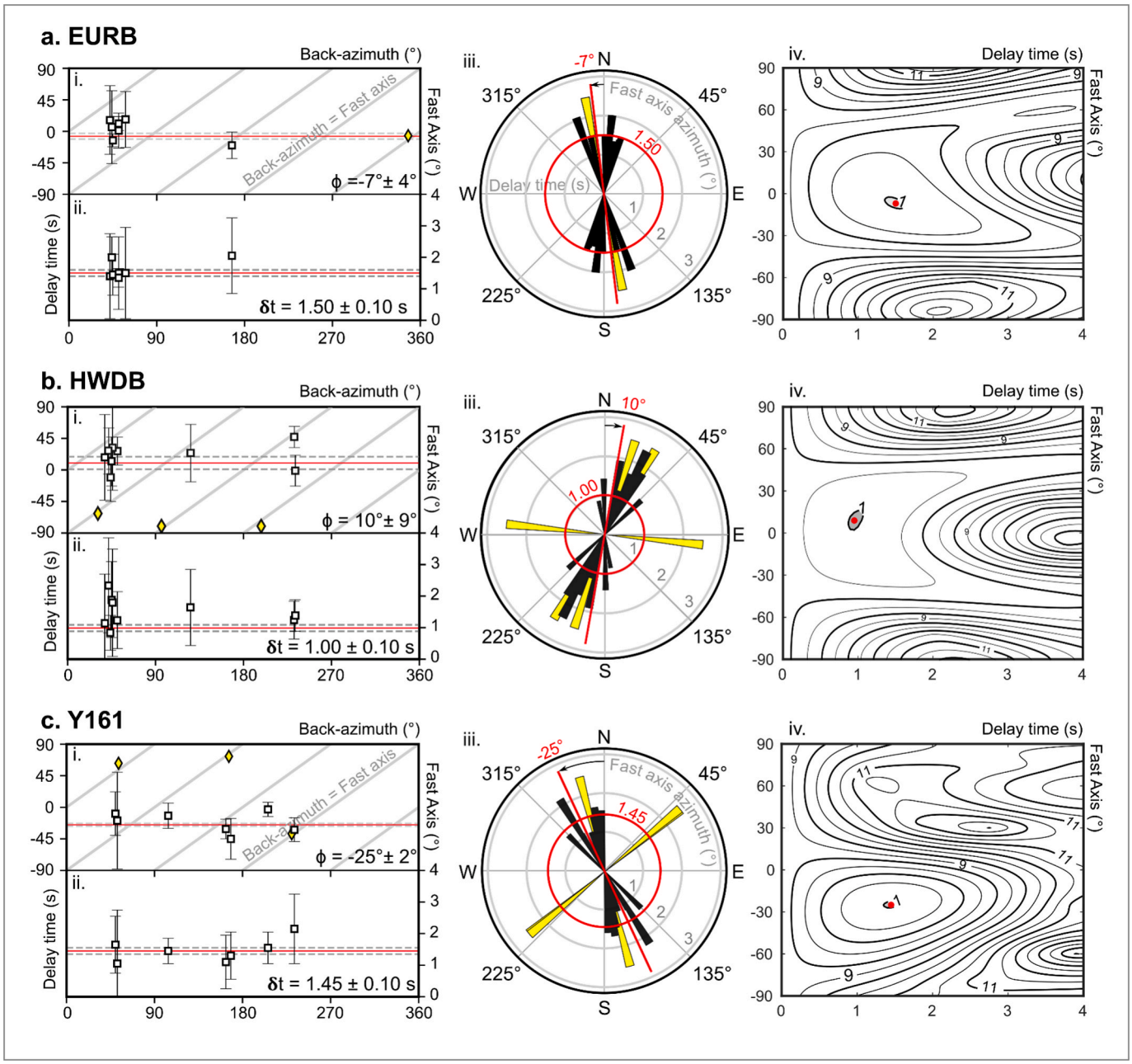

Fig. 7. Three examples of stacked and individual parameter analyses computed at stations (a) EURB, (b) HWDB, and (c) Y161. (i, ii) Individual fast axes and delay times (including their uncertainties) plotted against the back-azimuth. Squares and diamonds correspond to non-null and null observations, respectively. (iii) Rose diagrams showing individual non-null parameters (black bars) and null parameters (yellow bars), alongside their stacked values (red lines). (iv) Stacked contour levels. In all cases, red indicates the station-stacked parameters. The stacked-parameter uncertainties can be seen in i, ii, and iv. (For interpretation of the references to color in this figure legend, the reader is referred to the web version of this article.)

and slow shear-wave polarization directions, considering the angle of incidence of the observed *SK(K)S* phases through direction cosines (ray bending effects are not considered) and assuming an upper mantle density value of 3.4 g/cm^3 (Kennett et al., 1995). Since minerals are not perfectly aligned in real Earth volumes, we reduce the anisotropy effects in 50 % with respect to the ones calculated with the crystal elastic coefficients (Abt et al., 2009; Abt and Fischer, 2008). Finally, we time-shift and rotate the original synthetic waveforms according to the eigenvectors (polarization direction) and eigenvalues (phase velocities) of the Christoffel matrix to address the effects of the anisotropic layer (Fig. 11b). These modified synthetic waveforms are compared to the observed seismograms by calculating the cross-correlation coefficient (Fig. 11c), and are then used to implement the covariance method (Silver and Chan, 1991) to determine whether the observed splitting parameters are accurately recovered. We visually inspect alignment, amplitude, and phase consistency to assess the accuracy of our synthetic data, and consequently, the validity of our model.

In Fig. 12 we show the distribution of the cross-correlation coefficient values for a total of 707 observations (including nulls) with a signal-to-noise ratio greater than 2.5. We accurately retrieve the observed seismograms, with cross-correlation coefficients exceeding 0.75 in 71 % of the cases (see Fig. 12a). This result suggests that the estimated depth and orientation of seismic anisotropy are consistent with a single-layer anisotropic structure. Discrepancies between observed and synthetics may occur because we assume that the anisotropy only resides in the uppermost mantle without considering lower

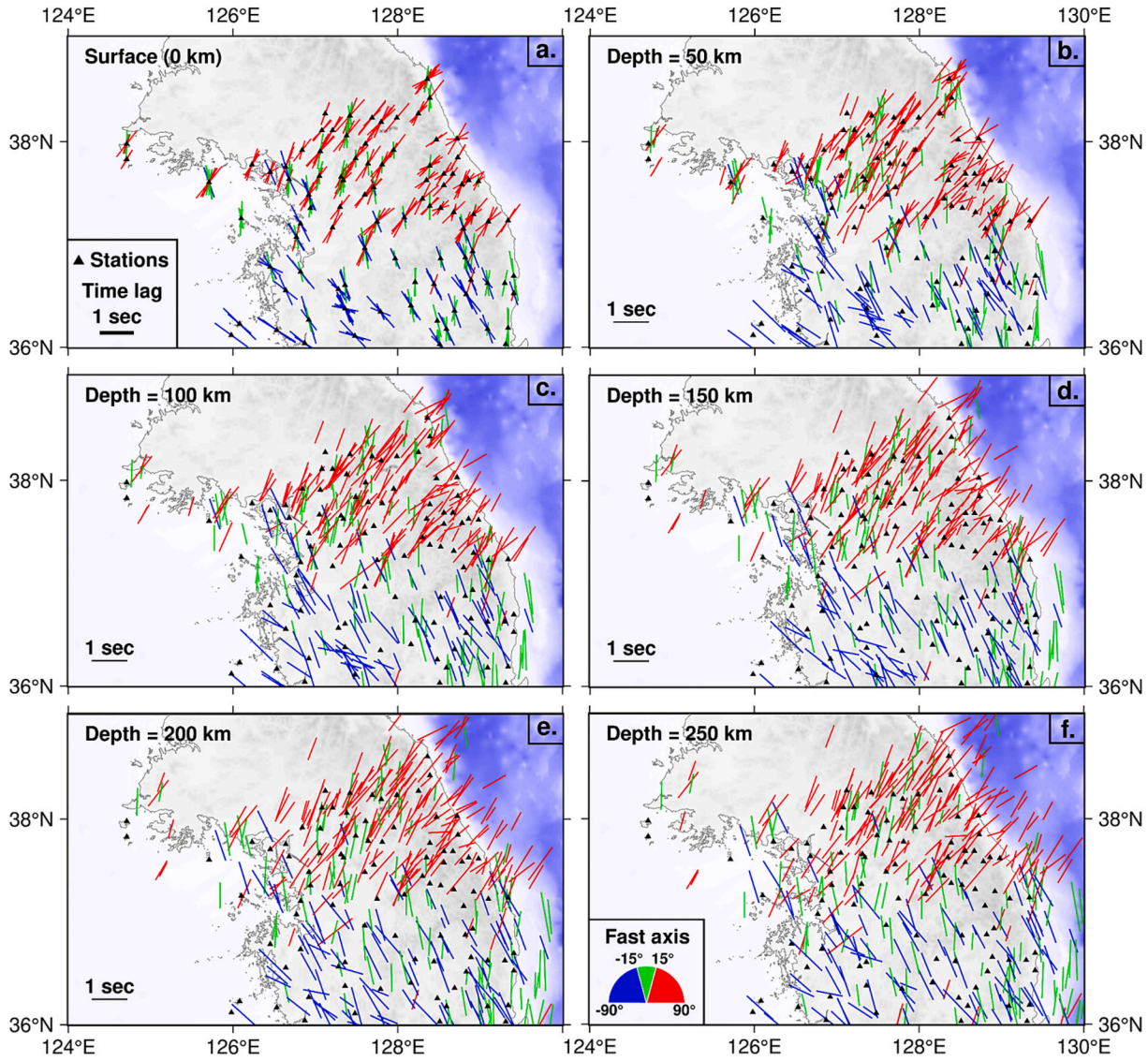

Fig. 8. Splitting parameters plotted at (a) surface and at piercing-point locations at (b) 50, (c) 100, (d) 150, (e) 200, and (f) 250 km depths. The bars are color coded according to legend and their length is defined by delay time.

mantle contributions, we consider an isotropic crust, we define a simple mineralogical composition to simulate the anisotropic layer, and we do not add noise to the synthetic seismograms. Another source of uncertainty may arise from the use of a single fast-axis direction for certain stations, despite evidence that anisotropy at depth exhibits lateral variations (see Figs. 8 and 9).

6. Discussion

We compare our measurements with recent seismic tomography models of the Korean Peninsula (Park and Hong, 2024b; Song et al., 2020) to discern the link of velocity anomalies in the upper mantle with core-refracted shear-wave anisotropy. There is a strong correlation between our *SK(K)S* fast axes and the Vs anomalies at depth, particularly at 60 km and 120 km (Fig. 13). This correlation, along with the observed delay times and the unimodal distribution of fast directions in most locations, suggests that the anisotropy beneath the region resides only in one layer, probably down to ~ 180 km, and could be interpreted in terms of both past and present dynamic processes in the upper mantle, and their connection to the Korean Peninsula's tectonic evolution.

In general, two main seismic velocity anomalies constitute the upper mantle structure beneath the Korean Peninsula (Song et al., 2020). A high-velocity structure beneath the central, western, and northwestern regions, and a low-velocity structure beneath the northeastern and eastern regions. The boundary between the anomalies is notably in agreement with the lateral variations of *SK(K)S* anisotropy that we observe, particularly along the limit between the Gyeonggi and Yeongnam massifs. Beneath the Gyeonggi massif, the Gyeongsang basin, and the eastern Korean Peninsula, a thermally elevated upper mantle has been proposed as the cause of low-velocity anomalies (Park and Hong, 2024b; Song et al., 2020), while beneath the Yeongnam massif and the western Korean Peninsula, a thick and remnant cratonic root has been interpreted as responsible of the high-velocity anomaly (Song et al., 2020). Our interpretation is guided by these structures and their association with tectonic episodes, as discussed in the following sections.

6.1. *Fast axes in the central region: Yeongnam massif and Gyeongsang basin (Region 1)*

In the central region, we observe fast axes oriented in the NW-SE direction that are approximately perpendicular to the predominant surface orientation of geological features (NE-SW), including the

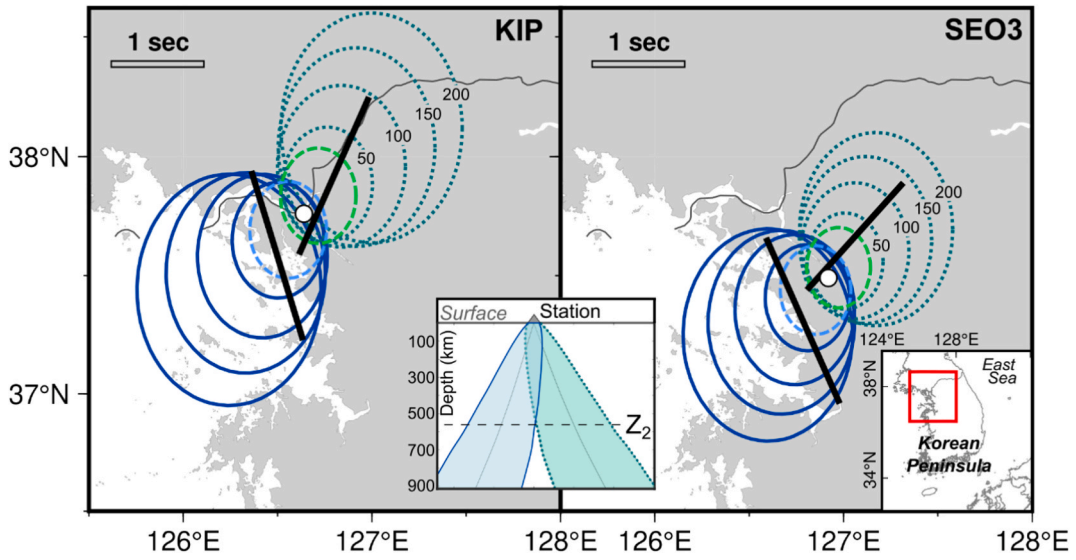

Fig. 9. Lateral variation of seismic anisotropy observed at stations KIP (left) and SEO3 (right) in the northwestern part of the study area (zoomed region shown in the bottom right inset). Two events with different back-azimuths show different splitting parameters at the same station. Dashed circles correspond to 35 km depth of the Fresnel zone, while the rest correspond to greater depths as shown in the figure. Centered inset shows a cross section for the two incoming *SKS* waves recorded at station SEO3. Left: Fresnel zones for two *SKKS* phases (back-azimuths: 45° and 231°) recorded at station KIP. Right: Fresnel zones for two *SKS* phases (back-azimuths: 51° and 233°) recorded at station SEO3. Dotted (green) and solid (blue) circles correspond to Fresnel zones of phases coming from the NE and SW, respectively. (For interpretation of the references to color in this figure legend, the reader is referred to the web version of this article.)

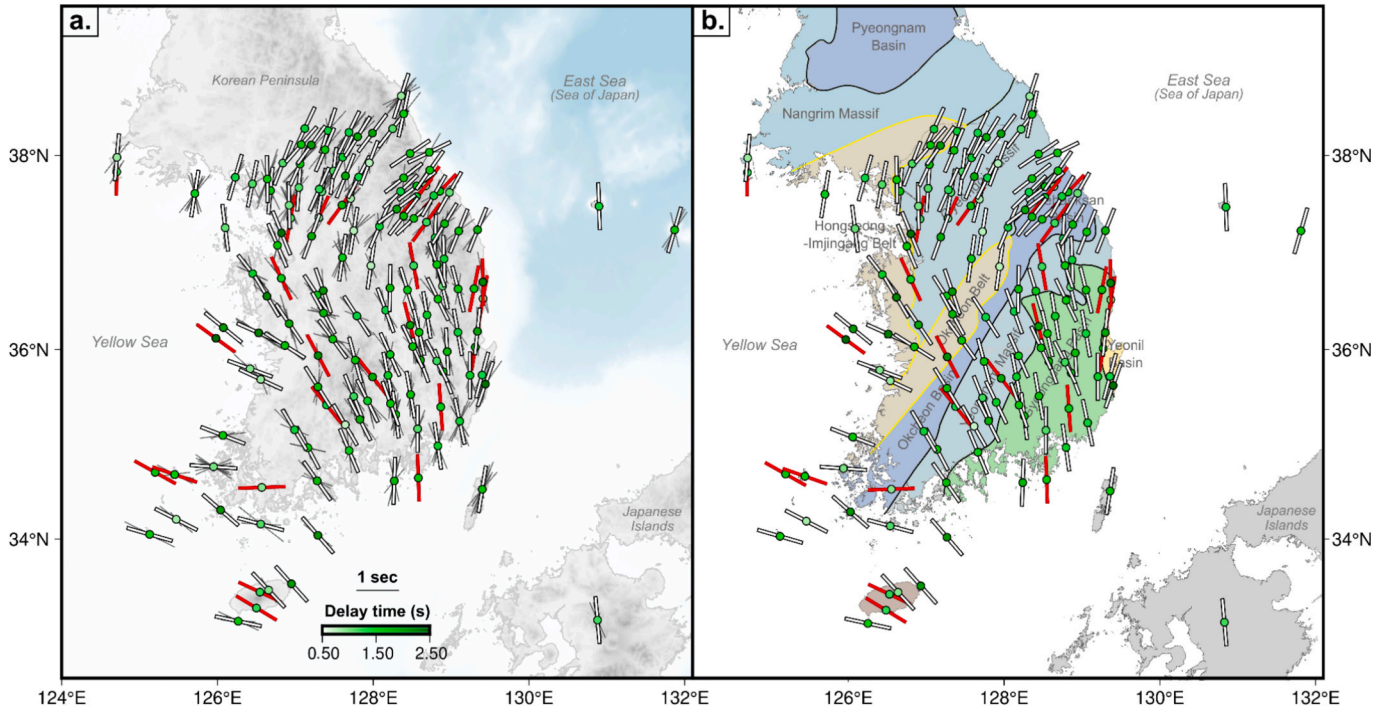

Fig. 10. Station-stacked shear-wave splitting parameters using the method of Wolfe and Silver (1998). Circles representing seismic stations are color-coded according to the stacked delay time. Bars are oriented according to the stacked fast direction. White bars indicate well-constrained measurements, whereas red bars represent poorly constrained and unconstrained parameters. (a) Stacked parameters plotted with their individual measurements in the background. (b) Correlation between stacked parameters and surface geology. (For interpretation of the references to color in this figure legend, the reader is referred to the web version of this article.)

Okcheon belt, the Yeongnam massif, and the Gyeongsang and Okcheon basins, and parallel to the past subduction direction (NW) of the paleo-Pacific plate (Chough et al., 2000; Kim et al., 2024) (Figs. 10 and 13). Here, our observations coincide with a high Vs anomaly that extends down to approximately 200 km depth (Song et al., 2020). The coherence of this velocity structure with surface geological expressions may suggest a strong coupling between the lithosphere and the sublithospheric mantle, or a deep lithospheric mantle (~180 km, based on our results). Both scenarios are common in ancient, stable continental regions (i.e., cratons) (Fouch and Rondenay, 2006). The Korean Peninsula is often classified as a stable intraplate environment with relatively low seismicity (e.g., Hong et al., 2015; Park et al., 2021), thus a strong

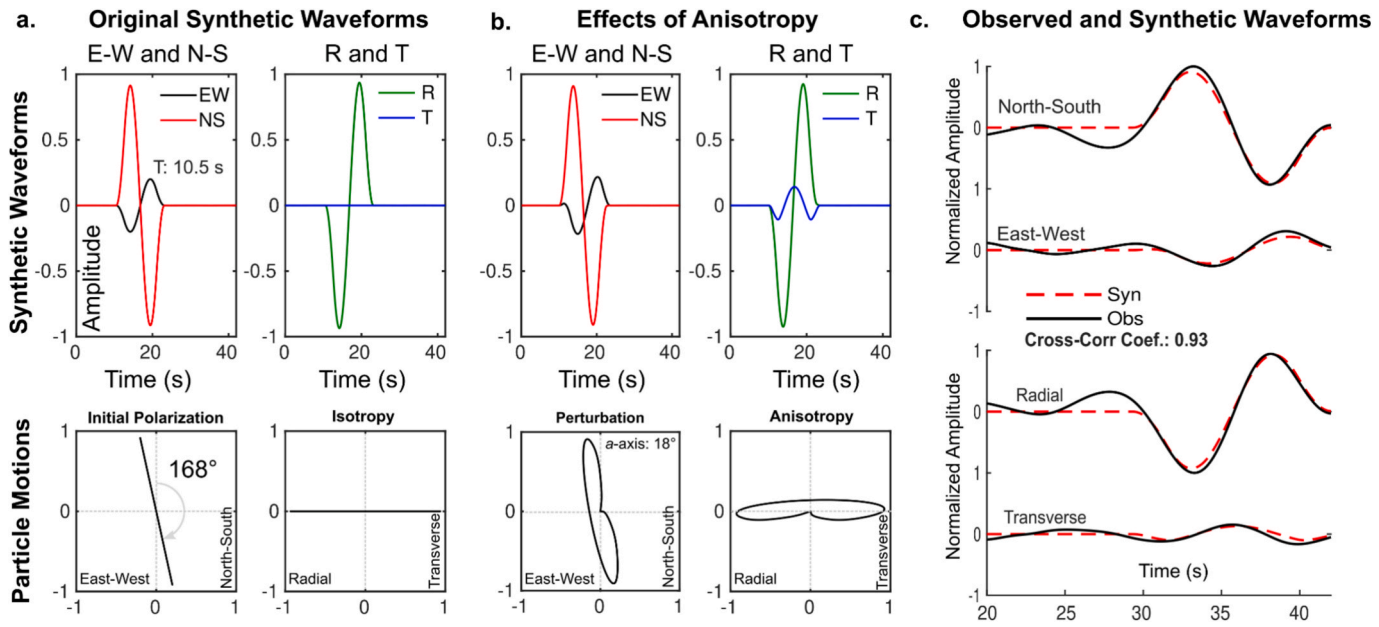

Fig. 11. Validation test example carried out for the *SKS* phase from the M_w 6.0 earthquake of July 23, 2019, recorded at station KOSB (KS) located in the northeastern part of the region. (a) Synthetic waveforms (top) and initial particle motions (bottom) based on the back-azimuth (~ 168°) and period (10.5 s) of the observed *SKS* phase. (b) Perturbed waveforms after their propagation through an anisotropic layer with a fast axis (18°) and thickness (95.2 km) defined by the station-stacked fast direction and delay time, respectively (see supplementary materials for more details), considering the incidence angle of the observed *SKS* phase (~ 8.30°). The energy on the transverse and the perturbed particle motions indicate anisotropy. (c) Comparison between observed and synthetic waveforms (more examples are provided in supplementary materials).

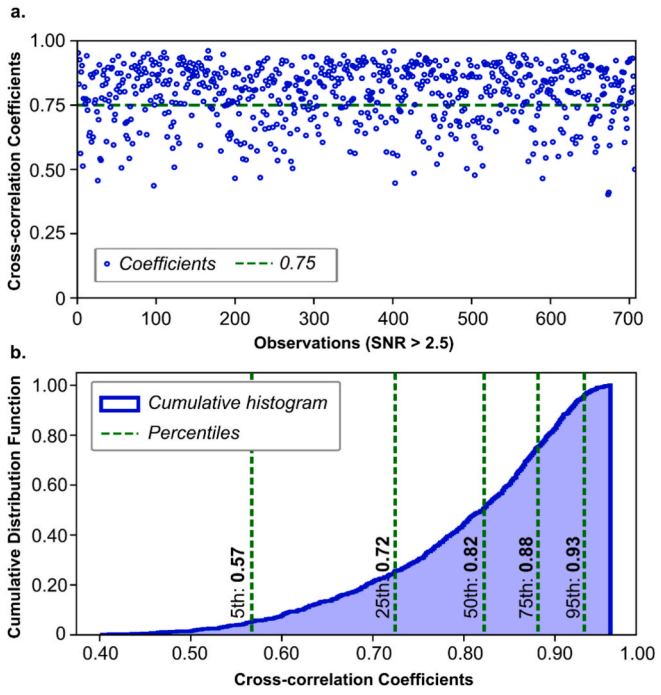

Fig. 12. Validation test results based on 707 observations with a signal-to-noise ratio (SNR) greater than 2.5. (a) Distribution of individual cross-correlation coefficient values. (b) Cumulative distribution function of the cross-correlation coefficients.

coupling between the asthenosphere and the lithosphere is likely to occur. Furthermore, the lithospheric thinning and extension and intraplate volcanism throughout the peninsula are probably indicative of strong lithosphere-asthenosphere coupling and coherent deformation (Ma et al., 2023).

In addition to being consistent with surface geological features and coinciding with a high-velocity anomaly, this fast-axis trend appears to terminate along the Okcheon belt, which separates the Gyeonggi and Yeongnam massifs (Fig. 10). These observations lead to two possible interpretations. (1) The most intuitive one is that the fast axes responded to the tectonic deformation process that gave rise to the current surface configuration, which means that we might be observing fossil anisotropy. According to Cheon et al. (2020), during the Early Cretaceous, the oblique subduction of the paleo-Pacific plate generated a NW-SE compressional stress field in the southeastern Korean Peninsula which may have caused the reorientation of the upper mantle minerals in the same direction, if A-type olivine fabric (or similar) is assumed. This scenario supports the formation of the Gyeongsang basin as a continental back-arc basin controlled by strike-slip movements induced by the oblique paleo-Pacific plate subduction (e.g., Cheon et al., 2020; Kim et al., 2016), and the formation of Jurassic granitoids in the southern Korean Peninsula due to an igneous activity induced by the same subduction process (Cheong and Jo, 2020; Kim et al., 2024). If the observed fast axes were reoriented in response to this subduction, then it would suggest that the subduction only affected the southeastern part of the peninsula, and it would be hard to correlate this region either with the North or South China blocks. (2) On the other hand, Song et al. (2020) interpret a cold, resistant cratonic lithosphere fragment extending downward to depths of 200 km, as mentioned above. This observation challenges the possibility that the paleo-Pacific plate subducted beneath the Korean Peninsula. Furthermore, since it suggests a thick lithosphere, it supports the interpretation that our core-refracted shear-wave splitting parameters reflect fossil fabrics within the intracratonic lithosphere, rather than anisotropy caused by a mantle flow deformation process. In this case, fossil anisotropy might reveal the direction of motion of the continental block when it was younger or during its formation. According to Chough et al. (2006, 2000) and Yin and Nie (1993), this region should be correlated with the North China block, with the South Korean Tectonic Line representing the collision boundary, whereas Choi et al. (2006), Kim et al. (2013), Oh (2006) and many others argue that it should be correlated with the South China block with the collision

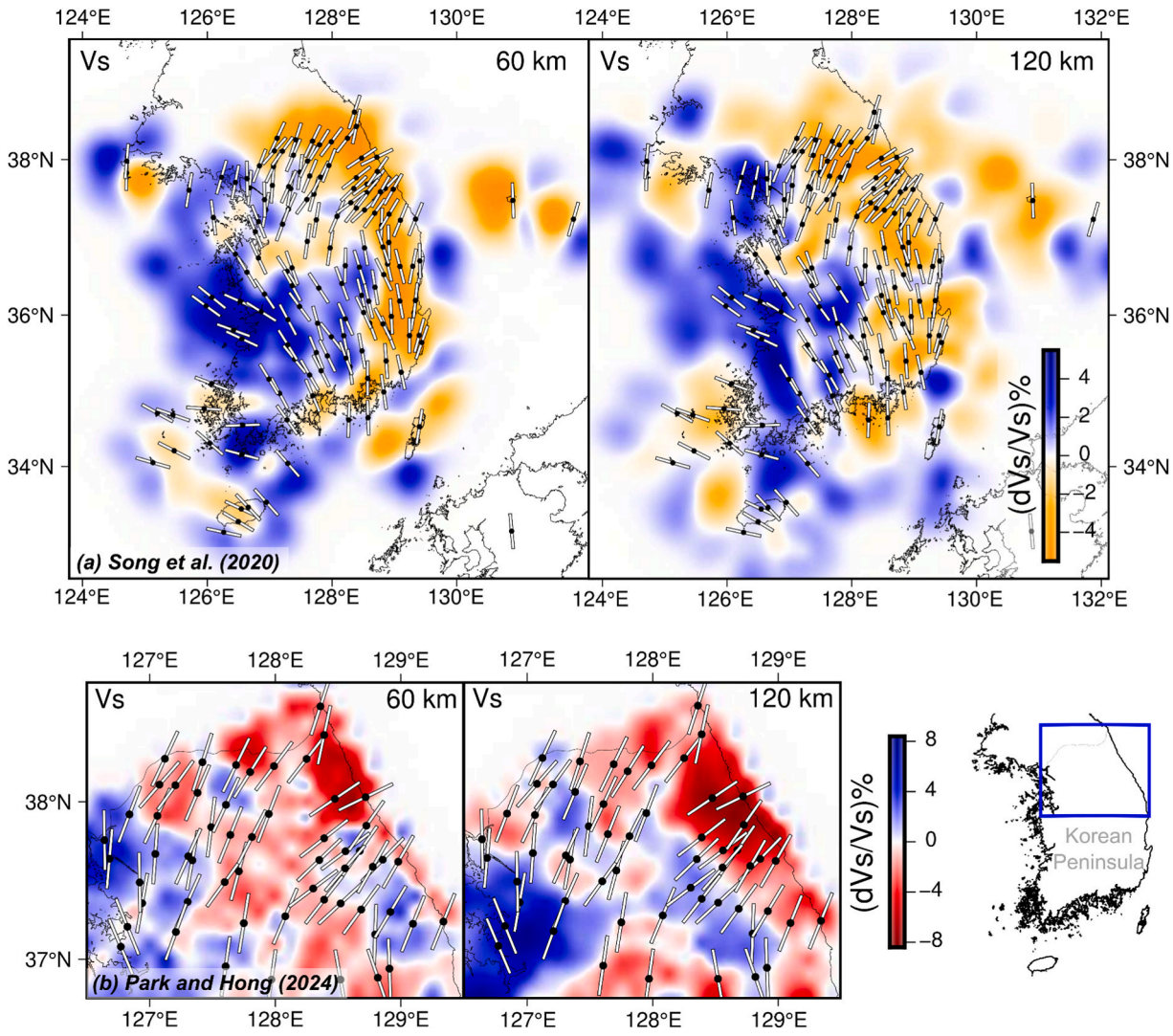

Fig. 13. Comparison of SK(K)S anisotropy with seismic tomography models by (a) Song et al. (2020) and (b) Park and Hong (2024b) at 60 km (left) and 120 km (right) depths. White bars represent the anisotropy results and are oriented according to ϕ. The bottom-right map indicates the region covered by the tomography in panel (b) (Park and Hong, 2024b).

boundary coinciding with the Hongseong-Odesan belt (e.g., Oh, 2006) or with the Imjingang belt (e.g., Kim et al., 2013). Since there is not enough evidence (such as the presence of eclogite facies or ultra-high metamorphic rocks) along the South Korean Tectonic Line and that we observe a clear fast polarization direction change coinciding with the Okcheon belt (Fig. 10), we believe that the upper mantle anisotropy is in agreement with those previously proposed collisional models where the tectonic boundary is located in central Korean Peninsula and not along the South Korean Tectonic Line.

In summary, the interpreted fossil anisotropy for this region can be linked either to the NW paleo-Pacific plate subduction, or to a preserved lithospheric anisotropy within the Yeongnam massif, although its tectonic affinity —whether to the North or South China block- remains uncertain. This latter scenario is the one that we support the most based on seismological evidence (Song et al., 2020). It is important to highlight that none of the scenarios support the NE migration of the South China block along the South Korean Tectonic Line (e.g., Chough et al., 2013, 2006; Li, 1994), which has been interpreted as the counterpart of the left-lateral strike-slip Tan-Lu fault in eastern China (Zhao et al., 2016, and references therein). For this reason, there is a possibility that this fragment of continental lithosphere has been deformed or rotated during the post-collisional period (i.e., after the Triassic). There is paleomagnetic evidence from the Gyeongsang basin indicating that the Korean Peninsula underwent significant clockwise rotation during the Cretaceous period (e.g., Lee et al., 2011; Uno, 2000). This rotation might have affected somehow the fast axes observed in this region.

To the west in the same region, in the southern part of the Hongseong-Imjingang belt, six stations exhibit a clockwise reorientation of *SK(K)S* fast axes (Fig. 10). Since these observations coincide with a strong high-velocity anomaly (Fig. 13), it is difficult to correlate them to post-collisional tectonic episodes. Thus, we believe that this rotation was directly related to a consequence of the collision between the North and South China blocks, which might have caused a change in mantle deformation style within the lithospheric root.

6.2. *Fast axes in the southwestern region: Jeju Volcanic Terrain and Yellow Sea (Region 2)*

Along the southwestern coast of the Korean Peninsula, *SK(K)S* anisotropy shows a counterclockwise rotation relative to the central region, with its fast axes oriented approximately in the WNW-ESE and E-W directions. In this second region, the anisotropy appears to respond to a more recent tectonic episode than the one that gave rise to the previous one. This interpretation is supported by the observed low-velocity

anomalies that become more pronounced with increasing depth (Fig. 13). Furthermore, these directions are not in agreement with any previously proposed collisional models, which is why we attribute them to a post-collisional tectonic process. We believe that there has been a post-collisional extension that led to the opening of the Yellow Sea basin. This spreading has been proposed by different authors (Kimura et al., 1990; Niu and Tang, 2016; Petrishchevsky, 2022) who suggested that it occurred long after the collision (ca. 27 Ma) but before the current subduction of the Philippine Sea plate (ca. 16 Ma), which likely caused its cessation (Niu and Tang, 2016). This extension (i.e., the Yellow Sea opening) could have caused the rotation or displacement of the southern part of the Korean Peninsula towards the east, affecting its current shape and probably reorientating upper mantle minerals in a direction parallel to the extension along and near the western coast (assuming A-type olivine fabric). It is worth mentioning that if the Jurassic subduction of the paleo-Pacific plate did occur (Chough et al., 2000; Kim et al., 2024), then there is a possibility that this fast-axis readjustment towards the E-W direction is related to the opening of the Yellow Sea as a back-arc basin in response to the subduction. However, the subduction direction remains unclear. In any case, these observations reflect fossil anisotropy, given that the extension in the Yellow Sea has ceased (Niu and Tang, 2016; Petrishchevsky, 2022).

In the Jeju Island area, we observe very few reliable measurements and many poorly constrained. We believe this might be due to a more complex anisotropic structure perhaps produced by a vertical mantle flow given that this island is thought to have formed as a result of volcanic activity (Brenna et al., 2015; Song et al., 2018). In case of vertical mantle flow, a low-velocity anomaly is expected and we would measure small or null delay times, which is consistent with our observations. In spite of the small number of measurements, they are remarkably consistent, and we believe they could respond to the Yellow Sea basin extension, as explained before, and/or to a trenchward mantle flow caused by the Philippine slab rollback as proposed by Brenna et al. (2015), since the fast axes are parallel to the slab motion direction (~NW) (Lallemand, 2016).

6.3. Fast axes in the southeastern Korean Peninsula (Region 3)

Along the southeastern coast of the Korean Peninsula, at stations in the Japanese archipelago, and on Dokdo and Ulleung islands, we observe fast axes oriented approximately in the N-S NE-SW directions, coinciding with a region characterized by a low-velocity anomaly (Fig. 13). Along the southeastern coast, we attribute the fast axis orientations to a direct consequence of the opening of the East Sea (Sea of Japan). Initially, the Korean Peninsula was connected to the southwestern Japanese Islands (before ca. 23 Ma) (Hisada et al., 2008; H. J. Kim et al., 2015). Subsequently, a back-arc rifting triggered a breakup and led to the clockwise rotation of the Japanese Islands away from the Korean Peninsula (Otofuji and Matsuda, 1987; Vaes et al., 2019). We propose that a thermally elevated upper mantle, marked by a low-velocity anomaly (Fig. 13), contributed to this back-arc rifting and induced the reorientation of minerals in both the lithospheric and asthenospheric mantle beneath the southeastern part of the peninsula. This observation supports models suggesting that the East Sea (Sea of Japan) was opened following a fan-shape (or bar-door) mechanism (e.g., Otofuji et al., 1985; Otofuji and Matsuda, 1987, 1983; Vaes et al., 2019), given that the fast axis directions exhibit a slight clockwise rotation relative to the ones observed inland in the Korean Peninsula. We believe that, since the center of this rifting process was located to the north (Park and Hong, 2024b), it may have caused a clockwise rotation of mantle minerals rather than a full reorientation in the direction of extension (E-W). Furthermore, it has been proposed that a subsequent back-arc spreading within the East Sea took place from Early to Middle Miocene in the NNW-SSE direction and caused the opening of the Ulleung basin (H. J. Kim et al., 2015). It is difficult to constrain its effect on the observed anisotropy, but this spreading episode may have affected the fast directions in the region and could explain the observed N-S and NE-SW trends of fast axes, instead of the expected E-W orientation.

On Ulleung and Dokdo islands, fast axes exhibit N-S and NE-SW fast axis orientations, respectively. These orientations could be explained based on the back-arc spreading episode described above (H. J. Kim et al., 2015). This episode may also suggest upwelling of underlying mantle material, inducing vertical mantle flow beneath the East Sea, as proposed by Yang et al. (2022). Furthermore, Chen et al. (2021) interpret the presence of a two-layer magma chamber beneath the Ulleung island, which is in agreement with the inferred vertical mantle flow beneath the East Sea. It is possible that magma upwelling has influenced the observations on this island (on average $\phi = -2^{\circ} \pm 14^{\circ}$, $\delta t = 1.25 \pm 0.25s$), which could account for the observed differences in splitting parameters between Ulleung and Dokdo islands. However, constraining the effects of vertical mantle flow on anisotropy is difficult due to technical limitations; therefore, additional data from more stations are required to substantiate these hypotheses.

At a single station located inland in southwestern Japan, we observe an average fast polarization direction of $\phi = -5^{\circ} \pm 24^{\circ}$, which is oblique to the direction of motion of the Philippine subducting slab (NW according to Gripp and Gordon, 2002) (see Fig. 1b). In the same region, Long and van der Hilst (2005) observe a rotation of fast axes from an orientation perpendicular to the direction of motion of the Philippine Sea plate to a direction parallel to it while going farther inland from the trench. Our trench-oblique observation agrees with this rotation since it falls in the middle part of the region. This rotation could be explained based on the transition from B-type (trench-parallel fast axes) to A-type (trench-normal fast axes) olivine fabrics while going away from the trench in a mantle wedge dominated by a 2-D corner flow (Karato, 2004; Kneller et al., 2005; Long and van der Hilst, 2005). The fast polarization directions observed at this station may be controlled by the subduction of the Philippine Sea plate, in contrast to the mechanisms that generated the upper mantle anisotropy in the southeastern Korean Peninsula.

6.4. Fast axes across the northern region

North of 37°N, from west to east, three different trends of fast axes are observed: N-S in the western part, NNE-SSW in the central part, and NE-SW in the eastern part. These trends are in good agreement with marked velocity contrasts (Fig. 13) and with geological expressions at surface (Fig. 10), which is why we believe they reveal many important aspects about the tectonic evolution that will be explained below.

Northwestern region. – Fast axes in the northwestern region are oriented approximately in the N-S direction and coincide with the Hongseong-Imjingang belt. As mentioned in the section on the tectonic framework, several authors have proposed that the collision boundary between the North and South China blocks is located along the West Marginal Fault Zone (Chang and Zhao, 2012; Hao et al., 2007; Hu et al., 2022; Kwon et al., 2009; Zhai et al., 2007) and/or along the Hongseong-Imjingang belt (Kim et al., 2013; Kwon et al., 2009; Sajeev et al., 2010) (Fig. 1a). Since fast axis orientations in this region are parallel to the Tan-Lu Fault in eastern China and are approximately perpendicular to the Sulu collision belt in the Shandong Peninsula (see Fig. 1a), we believe that they were produced in response to the northward migration of the South China Block when it collided against the North China Block. Furthermore, this N-S oriented trend broadly aligns with the location of a high-velocity anomaly and is delimited by the Hongseong-Imjingang belt, where a marked change in anisotropy parameters is observed while going westward into the Gyeonggi massif, as supported by piercing point and Fresnel zone analyses (Figs. 8 and 9). This lateral change is also consistent with a pronounced velocity contrast observed by Song et al. (2020) and Park and Hong (2024b) (Fig. 13). For these reasons, we strongly believe that the Hongseong-Imjingang belt constitutes a segment of the collision boundary between the North and South China blocks and that the Gyeonggi and Nangrim massifs should be

correlated to the North China Block. This explains high-pressure metamorphic rocks that have been found in the Hongseong Complex with ages similar to the eclogite facies observed along the Qinling-Dabie-Sulu belt to the west (Hu et al., 2022). It is worth noting that this anisotropy pattern suggests a strong coupling between the lithosphere and the sublithospheric mantle and that no post-collisional events (such as the possible Jurassic subduction of the paleo-Pacific plate and the Cenozoic openings of the East and Yellow Seas) have been capable of removing the Permo-Triassic anisotropy signature in this region.

North-central region. – The north-central region coincides with the western Gyeonggi massif and exhibits an overall fast axis oriented in the NNE-SSW direction, which is rotated ~ 20° clockwise relative to the trend observed to the west. We believe that our anisotropy fast axes in this region reveal the direction of motion of the North China Block when it collided against the South China Block, since they are consistent with the inferred migration of the North China Block (including the Shandong and Korean peninsulas) during the Triassic (e.g., Chough et al., 2013; Oh, 2006). However, there is a possibility that the fossil anisotropy within the lithospheric mantle corresponding to the Gyeonggi massif, which has been defined as an ancient craton that consists of Precambrian metamorphic rocks and Mesozoic granitoids (Lee et al., 2003), has been affected by a more recent tectonic episode since a low-velocity anomaly is observed in this region (Fig. 13). It is worth mentioning that the estimated depth of the lithosphere-asthenosphere boundary beneath the Gyeonggi massif is around 95 km (Lee, 2016), which is why fossil fabrics within the lithospheric mantle may have an important contribution to the accrued *SK(K)S* anisotropy measured at surface.

The anisotropy patterns of the northwestern and north-central regions agree with those previous models that identified the Hongseong-Imjingang belt as a potential collision boundary between the North and South China blocks (e.g., Kim et al., 2013; Kwon et al., 2009; Sajeev et al., 2010), but they also suggest that models proposing the collision boundary to be offshore in the Yellow Sea, far from the Hongseong-Imjingang belt (e.g., Chang and Zhao, 2012; Hao et al., 2007; Hu et al., 2022), should be revisited, and those wherein the Gyeonggi massif is correlated with the South China Block (e.g., Chough et al., 2006, 2000; Yin and Nie, 1993) should be discarded.

Northeastern region. – Farther east in the northern part of the region, we observe fast axes oriented in the NE-SW direction that exhibit another clockwise rotation (~20°) relative to those observed in the north-central region. These observations coincide with the Taebaeksan basin and with the eastern Gyeonggi massif (Figs. 1b and 10b), and align with the location of a low-velocity anomaly (Fig. 13). We interpret them to respond to a local effect in the upper mantle that occurred after the collision. This local effect is likely related to the opening of the East Sea (Sea of Japan), since this extensional tectonic episode could have strongly affected the upper mantle structure along the eastern coast of the Korean Peninsula (Park and Hong, 2024b; Song et al., 2020). Park and Hong (2024b) interpret the low-velocity structure as a solidified magma underplating beneath Moho and a Moho uplift both in response to continental rifting linked to the opening of the East Sea. On the other hand, Song et al. (2020) interpret it as a thermally elevated upper mantle that caused the reactivation of the cratonic margin by its interaction with convective mantle flow, which is also related to the same opening mechanism. Since our shear-wave fast axes are approximately parallel to the NE-SW extensional direction (and perpendicular to the rift axis) responsible for the opening of the East Sea, we suggest that these orientations are a direct consequence of this Cenozoic tectonic event. We believe that they are specifically related to the strain induced by magma underplating resulting from the interaction between the cratonic margin and an uplifted mantle, as evidenced by a strong low-velocity anomaly at around 120 km depth (Park and Hong, 2024b).

6.5. Tectonic model: Collision boundary

Our core-refracted shear-wave anisotropy model offers insights that can selectively support or challenge previously proposed tectonic models for the collision boundary between the North and South China blocks. Based on the previous discussion, we propose two possible collision boundaries that are illustrated in Fig. 14. Both models include the Hongseong-Imjingang belt as the continuation of the Sulu collisional belt in the Shandong Peninsula, since it is clear from our results. As mentioned above, some authors have identified the Hongseong-Imjingang belt as a part of the collision boundary (e.g., Kim et al., 2013; Kwon et al., 2009; Sajeev et al., 2010), although they interpret the entire Gyeonggi massif as belonging to the collision belt.

Beyond the Hongseong-Imjingang belt, the first scenario that we propose consists of a southward continuation of the collision boundary perhaps along the West Marginal Fault Zone (Fig. 14), which agrees with models proposed by Chang and Zhao (2012), Hao et al. (2007), Hong and Choi (2012), Hu et al. (2022), Kwon et al. (2009), and Zhai et al. (2007). This scenario implies that the whole Korean Peninsula should be correlated with the North China Block and that the differences that we observe from core-refracted shear-wave anisotropy would be due to post-collisional tectonic episodes, such as thermally elevated upper mantle in the northern part, paleo-Pacific subduction in the southern part, or effects caused by extensional episodes that led to the opening of the lateral basins. Furthermore, the post-collisional extension that opened the Yellow Sea may have removed the anisotropy produced by the northward migration of the South China Block in the southwestern part of the Korean Peninsula. On the other hand, the second scenario that we interpret from our results consists of a collision boundary within the Korean Peninsula approximately coinciding with the southern limit of the Gyeonggi massif (Fig. 14). This scenario can be clearly interpreted from our estimates since they can be divided into two main regions based on two different patterns: the NE-SW fast orientation to the north, and the NW-SE fast orientation to the south. This possibility implies that the Gyeonggi and Yeongnam massifs should be correlated with the North and South China blocks, respectively. The fast axis orientations observed for the former may reveal the overall direction of motion of the tectonic block, while those observed for the latter may have been affected by post-collisional effects, including paleo-subdcution and/or the extensional episodes that gave rise to the Yellow and East Seas. It is worth noting that probably the collision boundary in this second scenario coincides with the Okcheon Belt, but it is somewhat complicated to define it based on our technique due to resolution limitations.

The model that we propose is summarized in Fig. 14. This figure presents the two proposed scenarios for the Late Permian-Triassic collision, along with the Cenozoic rifting and spreading that opened the East Sea, and the Cenozoic post-collisional extension that was responsible for the opening of the Yellow Sea. The hypothesized location of SW Japanese Islands in the Late Oligocene is drew based on Hisada et al. (2008), Kim et al. (2007), Otofuji and Matsuda (1987), and Vaes et al. (2019).

7. Conclusions

We have presented core-refracted shear-wave anisotropy measurements to provide insights into upper mantle dynamics and lithospheric deformation beneath the Korean Peninsula. Our results reveal a strong coupling between the lithosphere and the sublithospheric mantle, both characterized by the presence of A-type olivine fabric. The observed complexity in anisotropy patterns strongly suggests that anisotropy resulting from past tectonic episodes has been preserved. This indicates that no recent significant tectonic event has been capable of completely overprinting or removing the pre-existing anisotropy.

The model presented herein is consistent with a collision boundary along the Hongseong-Imjingang belt, which represents the eastward continuation of the Qinling-Dabie-Sulu collisional belt in China. Based on our observations, we delineate two possible scenarios for its further extension: it might continue further south along the West Marginal Fault Zone, wherein the whole Korean Peninsula corresponds to the North

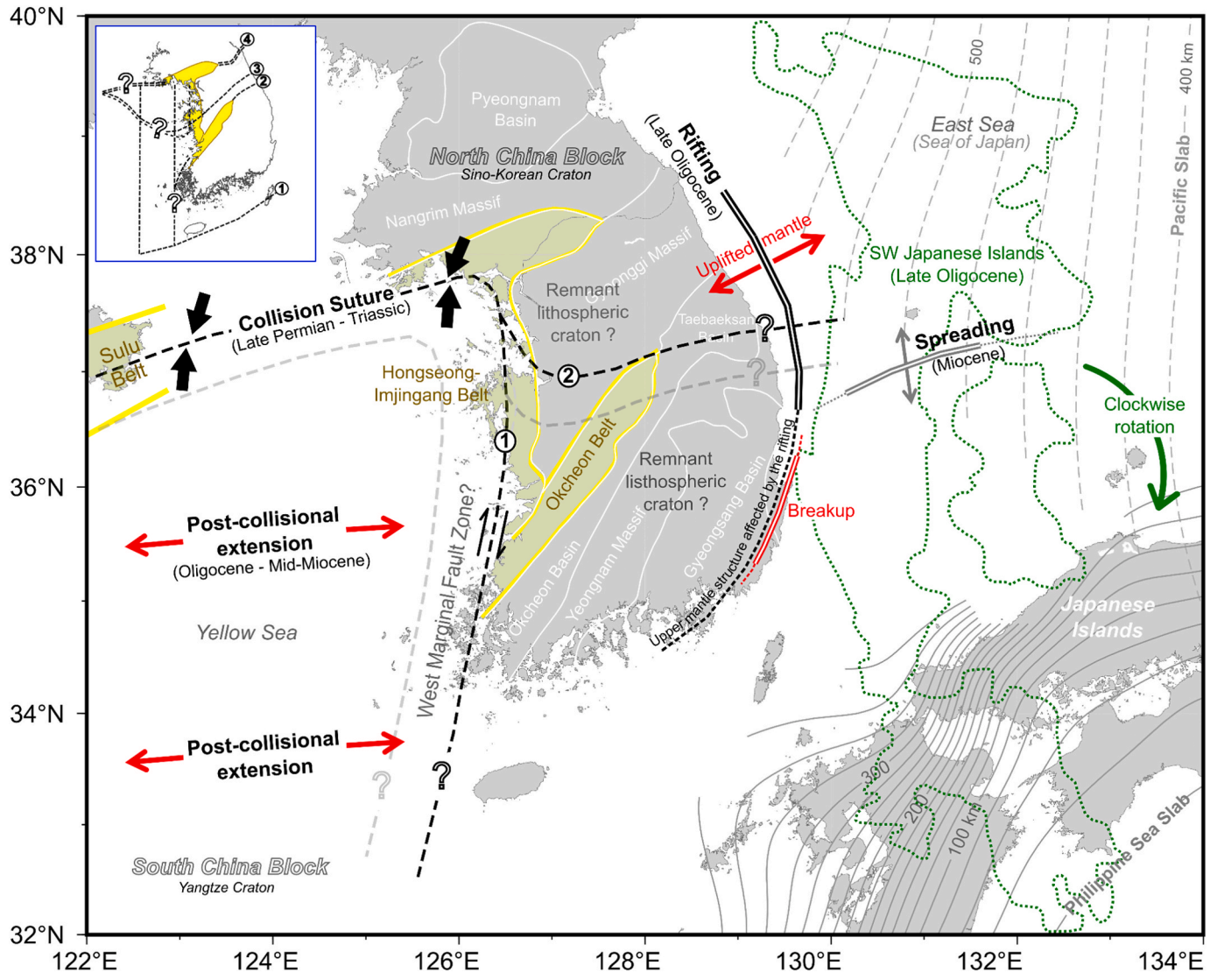

Fig. 14. Tectonic model. Two possible collision boundaries are interpreted (black dashed lines): (1) one along the Sulu-Hongseong-Imjingang belt that continues to the south along the West Marginal Fault Zone, and (2) another along the Sulu-Hongseong-Imjingang belt that continues to the east approximately coinciding with the southern boundary of the Gyeonggi massif. Black arrows indicate the segments of the collision suture where only one possible scenario is interpreted. The rifting (Late Oligocene) and spreading (Miocene) that yielded to the breakup and separation of SW Japanese Islands (green color) from the Korean Peninsula are indicated, as well as the clockwise rotation of the islands away from the peninsula (green arrow) (e.g., Hisada et al., 2008; Kim et al., 2007; Otofuji and Matsuda, 1987). The E-W post-collisional extension (Late Oligocene to Early Miocene) that we propose for the western region is also illustrated (red arrows within the Yellow Sea). For comparison, the top left inset shows previous models for the collision (see Fig. 1a for more details). (For interpretation of the references to color in this figure legend, the reader is referred to the web version of this article.)

China Block, or it might continue further east along the southern limit of the Gyeonggi massif.

We observe anisotropy patterns that we attribute to post-collisional tectonic episodes such as the opening of the Yellow and East Seas. Our model indicates that the Yellow Sea's opening is attributable to an approximately E-W extensional episode within the South China Block, while the East Sea's opening is linked to a clockwise rotation of the Japanese Islands away from the Korean Peninsula. This rotation likely began with an initial rifting episode that caused their breakup and continuous separation from the Korean Peninsula. Subsequently, a spreading episode may have caused their southeastward migration and the opening of the Ulleung basin in the East Sea.

The anisotropy patterns that we observe in the region corresponding to the Yeongnam and Gyeonggi massifs seem to respond to fossil anisotropy within remnant lithospheric cratons amalgamated before the collision. The observations in the western and central Gyeonggi massif probably reveal the true direction of motion of the North China Block when it collided with the South China Block, since it is consistent with previous studies. However, the fossil anisotropy that we observe in the Yeongnam massif does not align with the inferred direction of motion of either the North or South China blocks, which makes it hard to correlate this region with one of the two tectonic blocks. We believe that this anisotropy originates from a fossil fabric within the lithospheric craton dating from the time of its formation, although there is a possibility that it has been affected by post-collisional episodes involving subduction or rotation.

CRediT authorship contribution statement

Samuel Celis: Writing – original draft, Software, Formal analysis, Visualization, Methodology, Conceptualization, Writing – review & editing, Validation, Investigation. **Tae-Kyung Hong:** Supervision, Funding acquisition, Writing – review & editing, Resources, Conceptualization, Writing – original draft, Project administration. **Junhyung**

Lee: Funding acquisition, Investigation. **Seongjun Park:** Investigation, Funding acquisition, Supervision. **Yanbing Liu:** Investigation, Conceptualization, Validation. **Byeongwoo Kim:** Software, Data curation. **Jeongin Lee:** Software, Data curation. **Dong Geon Kim:** Data curation, Software.

Declaration of competing interest

The authors declare that they have no known competing financial interests or personal relationships that could have appeared to influence the work reported in this paper.

Acknowledgements

This work was supported by the Korea Meteorological Administration Research and Development Program under grant KMI2022-00710. Additionally, this research was partly supported by the Basic Science Research Program of National Research Foundation of Korea (NRF-2017R1A6A1A07915374). We thank Raúl W. Valenzuela for his insights on the technique. Lastly, we would like to express our sincere thanks to the Handling Editor Vasanthi Anthwar and to the two anonymous reviewers for their constructive suggestions and insightful comments that have significantly improved the clarity of our manuscript.

Data availability

The results of this study are available in the tables included in the supplementary materials. Original waveforms will be available on request.

Appendix A. Supplementary data

Supplementary data to this article can be found online at https://doi.org/10.1016/j.gr.2025.07.018.

References

Abramson, E.H., Brown, J.M., Slutsky, L.J., Zaug, J., 1997. The elastic constants of San Carlos olivine to 17 GPa. J. Geophys. Res. Solid Earth 102, 12253–12263. https://doi.org/10.1029/97JB00682.

Abt, D.L., Fischer, K.M., 2008. Resolving three-dimensional anisotropic structure with shear wave splitting tomography. Geophys. J. Int. 173, 859–886. https://doi.org/10.1111/j.1365-246X.2008.03757.x.

Abt, D.L., Fischer, K.M., Abers, G.A., Strauch, W., Protti, J.M., González, V., 2009. Shear wave anisotropy beneath Nicaragua and Costa Rica: Implications for flow in the mantle wedge. Geochem., Geophys. Geosyst. 10. https://doi.org/10.1029/2009GC002375.

Alsina, D., Sneider, R., 1995. Small scale sublithospheric continental deformation: constraints from SKS splitting observations. Geophys. J. Int. 123, 431–448.

Anderson, O.L., Isaak, D.G., 1995. Elastic Constants of Mantle Minerals at High Temperature, in: Mineral Physics \& Crystallography. American Geophysical Union (AGU), pp. 64–97. Doi: Doi: 10.1029/RF002p0064.

Babuska, V., Cara, M., 1991. Seismic anisotropy in the Earth. Springer Science and Business Media, Netherlands.

Barruol, G., Mainprice, D., 1993. A quantitative evaluation of the contribution of crustal rocks to the shear-wave splitting of teleseismic SKS waves. Phys. Earth Planet. In. 78, 281–300. https://doi.org/10.1016/0031-9201(93)90161-2.

Bowman, J.R., Ando, M., 1987. Shear-wave splitting in the upper-mantle wedge above the Tonga subduction zone. Geophys. J. R. Astron. Soc. 88, 25–41.

Brenna, M., Cronin, S.J., Kereszturi, G., Sohn, Y.K., Smith, I.E.M., Wijbrans, J., 2015. Intraplate volcanism influenced by distal subduction tectonics at Jeju Island, Republic of Korea. Bull. Volcanol. 77. https://doi.org/10.1007/s00445-014-0896-5.

Chang, K.H., Zhao, X., 2012. North and South China suturing in the east end: what happened in Korean Peninsula? Gondw. Res. 22, 493–506. https://doi.org/10.1016/j.gr.2011.12.010.

Chen, S.S., Lee, S.G., Simutė, S., Fichtner, A., Lee, T.J., Lee, Y.S., Liu, J.Q., Gao, R., 2021. Geochemical and seismic tomography constraints of two-layer magma chambers beneath the bimodal volcanism: a case study of late Cenozoic volcanic rocks from Ulleung Island and Mt. Changbai (Paektu). Chem. Geol. 581. https://doi.org/10.1016/j.chemgeo.2021.120386.

Cheon, Y., Ha, S., Lee, S., Son, M., 2020. Tectonic evolution of the cretaceous Gyeongsang Back-arc Basin, SE Korea: transition from sinistral transtension to strike-slip kinematics. Gondw. Res. 83, 16–35. https://doi.org/10.1016/j.gr.2020.01.012.

Cheong, A.C., Jo, H.J., 2017. Crustal evolution in the Gyeongsang Arc, Southeastern Korea: geochronological, geochemical and Sr-Nd-Hf isotopic constraints from granitoid rocks. Am. J. Sci. 317, 369–410. https://doi.org/10.2475/03.2017.03.

Cheong, A.C., Sik, Jo, H.J., 2020. Tectonomagmatic evolution of a Jurassic Cordilleran flare-up along the Korean Peninsula: Geochronological and geochemical constraints from granitoid rocks. Gondw. Res. 88, 21–44. https://doi.org/10.1016/j.gr.2020.06.025.

Choi, H., Hong, T.K., He, X., Baag, C.E., 2012. Seismic evidence for reverse activation of a paleo-rifting system in the East Sea (Sea of Japan). Tectonophysics 572–573, 123–133. https://doi.org/10.1016/j.tecto.2011.12.023.

Choi, S., Oh, C.-W., Luehr, H., 2006. Tectonic link between NE China and Korean Peninsula, revealed by interpreting CHAMP satellite magnetic and GRACE satellite gravity data. J. Korean Geophys. Soc. 9, 209–2017.

Chough, S.K., Kim, H., Woo, J., Lee, H.S., 2006. Tectonic implications of quartzite-shale and phyllite beds in the Seochangri Formation (Okcheon Group), Bonghwajae section, mid-Korea. Geosci. J. 10, 403–421. https://doi.org/10.1007/BF02910435.

Chough, S.K., Kwon, S.T., Ree, J.H., Choi, D.K., 2000. Tectonic and sedimentary evolution of the Korean peninsula: a review and new view. Earth Sci. Rev. 52, 175–235. https://doi.org/10.1016/S0012-8252(00)00029-5.

Chough, S.K., Lee, D.J., Ree, J.H., 2013. Whereabouts of the collision belt between the Sino-Korean and South China blocks in the northeast Asian margin. Geosci. J. 17, 397–401. https://doi.org/10.1007/s12303-013-0057-4.

Chough, S.K., Sohn, Y.K., 2010. Tectonic and sedimentary evolution of a cretaceous continental arc-backarc system in the Korean peninsula: New view. Earth-Sci. Rev. 101, 225–249. https://doi.org/10.1016/j.earscirev.2010.05.004.

Christensen, U., 1984. Convection with pressure- and temperature- dependent non-Newtonian rheology. Geophys. J. r. Astrc. Soc. 77, 343–384.

Cluzel, D., Cadet, J.P., Lapierre, H., 1990. Geodynamics of the Ogcheon Belt (South Korea). Tectonophysics 183, 41–56. https://doi.org/10.1016/0040-1951(90)90187-D.

Cluzel, D., Jolivet, L., Cadet, J.-P., 1991. Early middle paleozoic intraplate orogeny in the ogcheon belt (South Korea): a new insight on the paleozoic buildup of east Asia. Tectonics 10, 1130–1151.

Crampin, S., 1994. The fracture criticality of crustal rocks. Geophys. J. Int. 118, 428–438.

Fischer, K.M., Parmentier, E.M., Stine, A.R., Wolf, E.R., 2000. Modeling anisotropy and plate-driven flow in the Tonga subduction zone back arc. J. Geophys. Res. Solid Earth 105, 16181–16191. https://doi.org/10.1029/1999JB900441.

Fouch, M.J., Fischer, K.M., 1996. Mantle anisotropy beneath northwest Pacific subduction zones. J. Geophys. Res. 101, 15987–16002.

Fouch, M.J., Rondenay, S., 2006. Seismic anisotropy beneath stable continental interiors. Phys. Earth Planet. In. 158, 292–320. https://doi.org/10.1016/j.pepi.2006.03.024.

Fournier, M., Jolivet, L., Fabbri, O., 1995. Neogene stress field in SW Japan and mechanism of deformation during the Sea of Japan opening. J. Geophys. Res. 100, 295–314. https://doi.org/10.1029/95jb01973.

Frisillo, A.L., Barsch, G.R., 1972. Measurement of single-crystal elastic constants of bronzite as a function of pressure and temperature. J. Geophys. Res. 77, 6360–6384. https://doi.org/10.1029/JB077i032p06360.

Gripp, A.E., Gordon, R.G., 2002. Young tracks of hotspots and current plate velocities. Geophys. J. Int. 150, 321–361. https://doi.org/10.1046/j.1365-246X.2002.01627.x.

Hao, T.Y., Xu, Y., Suh, M., Xu, Y., Liu, J.H., Zhang, L.L., Dai, M.G., 2007. East marginal fault of the Yellow Sea: a part of the conjunction zone between Sino-Korea and Yangtze Blocks? Geol. Soc. Spec. Publ. 280, 281–292. https://doi.org/10.1144/SP280.14.

Helffrich, G., 1995. Lithospheric deformation inferred from teleseismic shear wave splitting observations in the United Kingdom. J. Geophys. Res. 100, 18195–18204. https://doi.org/10.1029/95jb01572.

Hisada, K.I., Takashima, S., Arai, S., Lee, Y.I.L., 2008. Early cretaceous paleogeography of Korea and Southwest Japan inferred from occurrence of detrital chromian spinels. Isl. Arc 17, 471–484. https://doi.org/10.1111/j.1440-1738.2008.00638.x.

Hong, T.K., 2010. Lg attenuation in a region with both continental and oceanic environments. Bull. Seismol. Soc. Am. 100, 851–858. https://doi.org/10.1785/0120090057.

Hong, T.K., Choi, H., 2012. Seismological constraints on the collision belt between the North and South China blocks in the Yellow Sea. Tectonophysics 570–571, 102–113. https://doi.org/10.1016/j.tecto.2012.08.034.

Hong, T.K., Kang, T.S., 2009. Pn travel-time tomography of the paleo-continental-collision and rifting zone around Korea and Japan. Bull. Seismol. Soc. Am. 99, 416–421. https://doi.org/10.1785/0120080120.

Hong, T.K., Lee, J., Houng, S.E., 2015. Long-term evolution of intraplate seismicity in stress shadows after a megathrust. Phys. Earth Planet. In. 245, 59–70. https://doi.org/10.1016/j.pepi.2015.05.009.

Hong, T.K., Lee, J., Lee, J., Park, S., Kim, B., Choi, S., 2023. Unravelling a midcrustal seismogenic fault structure from a seismic sequence and geophysical data: Application to the 28 October 2022 ML4.1 Goesan earthquake in the central Korean Peninsula. Geophys. J. Int. 235, 1117–1129. https://doi.org/10.1093/gji/ggad292.

Hong, T.K., Park, S., Lee, J., Kim, W., 2020. Spatiotemporal Seismicity Evolution and Seismic Hazard Potentials in the Western East Sea (Sea of Japan). Pure Appl. Geophys. 177, 3761–3774. https://doi.org/10.1007/s00024-020-02479-z.

Hong, T.K., Park, S., Lee, J., Lee, J., Kim, B., 2024. Middle to lower crustal earthquakes in the western East Sea (Sea of Japan) and their implications for neotectonic evolution. Tectonophysics 880. https://doi.org/10.1016/j.tecto.2024.230346.

Hu, P., Yang, F., Li, S., Zhang, R., Ni, B., Qiu, E., Suo, Y., 2022. Opposite thrust systems under the Subei-South Yellow Sea Basin: a synthesis on the closure of the eastern Tethyan Ocean. Earth-Sci. Rev. 231, 104075. https://doi.org/10.1016/j.earscirev.2022.104075.

Jang, Y., Kim, S.W., Samuel, V.O., Kwon, S., Park, S.I., Santosh, M., Yi, K., 2024. Paleozoic tectonic evolution of the proto-Korean Peninsula along the East asian continental margin from detrital zircon U-Pb geochronology and Hf isotope geochemistry. Geosci. Front. 15, 101700. https://doi.org/10.1016/j.gsf.2023.101700.

Jolivet, L., Tamaki, K., Fournier, M., 1994. Japan Sea, opening history and mechanism: a synthesis. J. Geophys. Res. 99, 22237–22259. https://doi.org/10.1029/93jb03463.

Jung, H., Katayama, I., Jiang, Z., Hiraga, T., Karato, S., 2006. Effect of water and stress on the lattice-preferred orientation of olivine. Tectonophysics 421, 1–22. https://doi.org/10.1016/j.tecto.2006.02.011.

Kano, K., Yoshikawa, T., Yanagisawa, Y., Ogasawara, K., Danhara, T., 2002. An unconformity in the early Miocene syn-rifting succession, northern Noto Peninsula, Japan: evidence for short-term uplifting precedent to the rapid opening of the Japan Sea. Isl. Arc 11, 170–184. https://doi.org/10.1046/j.1440-1738.2002.00363.x.

Karato, S.-I., Jung, H., Katayama, I., Skemer, P., 2008. Geodynamic significance of seismic anisotropy of the upper mantle: New insights from laboratory studies. Annu. Rev. Earth Planet. Sci. 36, 59–95. https://doi.org/10.1146/annurev.earth.36.031207.124120.

Karato, S.I., 2004. Mapping water content in the upper mantle. Geophys. Monogr. Ser. 138, 135–152. https://doi.org/10.1029/138GM08.

Kawaguchi, K., Oh, C.W., Jeong, J.W., Furusho, M., Shibata, S., Hayasaka, Y., 2023. Zircon U–Pb ages and Lu–Hf isotopes of the Jurassic Granites on the east coast of the Korean Peninsula and Southwest Japan: Petrogenesis and tectonic correlation between the Korean Peninsula and Japanese Islands. Gondw. Res. 117, 56–85. https://doi.org/10.1016/j.gr.2023.01.005.

Kee, W.-S., Kim, S.W., Kim, H., Hong, P., Kwon, C.W., Lee, H.-J., Cho, D.-L., Koh, H.J., Song, K.-Y., Byun, U.H., Jang, Y., Lee, B.C., 2019. Geologic Map of Korea (1: 1,000,000). Korea Institute of Geoscience and Mineral Resources.

Kee, W.S., Kim, S.W., Jeong, Y.J., Kwon, S., 2010. Characteristics of Jurassic continental arc magmatism in South Korea: Tectonic implications. J. Geol. 118, 305–323. https://doi.org/10.1086/651503.

Kennett, B.L.N., Engdahl, E.R., Buland, R., 1995. Constraints on seismic velocities in the Earth from traveltimes. Geophys. J. Int. 122, 108–124. https://doi.org/10.1111/j.1365-246X.1995.tb03540.x.

Kim, H.J., Lee, G.H., Choi, D.L., Jou, H.T., Li, Z., Zheng, Y., Kim, G.Y., Lee, S.H., Kwon, Y. K., 2015a. Back-arc rifting in the Korea Plateau in the East Sea (Japan Sea) and the separation of the southwestern Japan Arc from the Korean margin. Tectonophysics 638, 147–157. https://doi.org/10.1016/j.tecto.2014.11.003.

Kim, H.J., Lee, G.H., Jou, H.T., Cho, H.M., Yoo, H.S., Park, G.T., Kim, J.S., 2007. Evolution of the eastern margin of Korea: Constraints on the opening of the East Sea (Japan Sea). Tectonophysics 436, 37–55. https://doi.org/10.1016/j.tecto.2007.02.014.

Kim, J., Yi, K., Jeong, Y.J., Cheong, C.S., 2011. Geochronological and geochemical constraints on the petrogenesis of mesozoic high-k granitoids in the central korean peninsula. Gondw. Res. 20, 608–620. https://doi.org/10.1016/j.gr.2010.12.005.

Kim, J.H., 1996. Mesozoic tectonics in Korea. J. SE Asian Earth Sci. 13, 251–265. https://doi.org/10.1016/0743-9547(96)00032-3.

Kim, S.W., Kee, W.S., Lee, S.R., Santosh, M., Kwon, S., 2013. Neoproterozoic plutonic rocks from the western Gyeonggi massif, South Korea: Implications for the amalgamation and break-up of the Rodinia supercontinent. Precambr. Res. 227, 349–367. https://doi.org/10.1016/j.precamres.2012.01.014.

Kim, S.W., Kwon, S., Jeong, Y.J., Kee, W.S., Lee, B.C., Byun, U.H., Ko, K., Cho, D.L., Hong, P.S., Park, S.I., Santosh, M., 2021. The Middle Permian to Triassic tectono-magmatic system in the southern Korean Peninsula. Gondw. Res. 100, 302–322. https://doi.org/10.1016/j.gr.2020.11.017.

Kim, S.W., Kwon, S., Ko, K., Yi, K., Cho, D.L., Kee, W.S., Kim, B.C., 2015b. Geochronological and geochemical implications of Early to Middle Jurassic continental adakitic arc magmatism in the Korean Peninsula. Lithos 227, 225–240. https://doi.org/10.1016/j.lithos.2015.04.012.

Kim, S.W., Kwon, S., Park, S.I., Lee, C., Cho, D.L., Lee, H.J., Ko, K., Kim, S.J., 2016. SHRIMP U–Pb dating and geochemistry of the cretaceous plutonic rocks in the Korean Peninsula: a new tectonic model of the cretaceous Korean Peninsula. Lithos 262, 88–106. https://doi.org/10.1016/j.lithos.2016.06.027.

Kim, S.W., Lee, B.Y., Lee, S.H., Kee, W.S., Santosh, M., Ko, K., 2024. Early to Middle Jurassic (ca. 182–164 Ma) fractionated granitoids in the Korean Peninsula: Implication for the tectonomagmatic history of East Asia. Gondw. Res. 125, 229–252. https://doi.org/10.1016/j.gr.2023.08.017.

Kim, S.W., Oh, C.W., Williams, I.S., Rubatto, D., Ryu, I.C., Rajesh, V.J., Kim, C.B., Guo, J., Zhai, M., 2006. Phanerozoic high-pressure eclogite and intermediate-pressure granulite facies metamorphism in the Gyeonggi Massif, South Korea: Implications for the eastward extension of the Dabie-Sulu continental collision zone. Lithos 92, 357–377. https://doi.org/10.1016/j.lithos.2006.03.050.

Kimura, G., Takahashi, M., Kono, M., 1990. Mesozoic collision-extrusion tectonics in eastern Asia. Tectonophysics 181, 15–23. https://doi.org/10.1117/12.2324709.

Kimura, G., Tamaki, K., 1986. Collision, rotation, and back-arc spreading in the region of the Okhotsk and Japan seas. Tectonics 5, 389–401.

Kneller, E.A., van Keken, P.E., Karato, S.I., Park, J., 2005. B-type olivine fabric in the mantle wedge: Insights from high-resolution non-Newtonian subduction zone models. Earth Planet. Sci. Lett. 237, 781–797. https://doi.org/10.1016/j.epsl.2005.06.049.

Kwon, S., Kim, S.W., Santosh, M., 2013. Multiple generations of mafic-ultramafic rocks from the Hongseong suture zone, western South Korea: Implications for the geodynamic evolution of NE Asia. Lithos 160–161, 68–83. https://doi.org/10.1016/j.lithos.2012.11.011.

Kwon, S., Sajeev, K., Mitra, G., Park, Y., Kim, S.W., Ryu, I.C., 2009. Evidence for Permo-Triassic collision in Far East Asia: the Korean collisional orogen. Earth Planet. Sci. Lett. 279, 340–349. https://doi.org/10.1016/j.epsl.2009.01.016.

Lallemand, S., 2016. Philippine Sea Plate inception, evolution, and consumption with special emphasis on the early stages of Izu-Bonin-Mariana subduction. Prog. Earth Planet Sci. 3. https://doi.org/10.1186/s40645-016-0085-6.

Lallemand, S., Jolivet, L., 1986. Japan Sea: a pull-apart basin? Earth Planet Sci. Lett. 76, 375–389. https://doi.org/10.1016/0012-821X(86)90088-9.

Lee, B.Y., Oh, C.W., Cho, D.L., Zhai, M., Lee, B.C., Peng, P., Yi, K., 2019. The Devonian back-arc basin and Triassic arc-continent collision along the Imjingang belt in the Korean Peninsula and their tectonic meaning. Lithos 328–329, 276–296. https://doi.org/10.1016/j.lithos.2019.01.011.

Lee, Y.I., Kim, J.Y., 2005. Provenance of the Hayang Group (Early cretaceous) in the Yeongyang Subbasin, SE Korea and its bearing on the cretaceous palaeogeography of SW Japan. Palaeogeogr. Palaeoclimatol. Palaeoecol. 228, 278–295. https://doi.org/10.1016/j.palaeo.2005.06.017.

Lee, Y.I., Lee, J.I., Choi, Y.S., 2023. Provenance analysis of the cretaceous Gyeongsang Basin, SE Korea: a synthesis and tectonic implications for active continental margin in East Asia. Earth-Sci. Rev. 238, 104334. https://doi.org/10.1016/j.earscirev.2023.104334.

Lee, J., Hong, T.K., Park, S., Kim, B., 2024. Midcrustal moderate-size earthquake occurrence in paleovolcanic structures off Jeju Island, South Korea. Phys. Earth Planet. Inter. 352, 107210. https://doi.org/10.1016/j.pepi.2024.107210.

Lee, J.I.L., Lee, Y.I.L., 2000. Provenance of the lower cretaceous hayang group, gyeongsang basin, southeastern korea: Implications for continental-arc volcanism. J. Sediment. Res. 70, 151–158. https://doi.org/10.1306/2DC40906-0E47-11D7-8643000102C1865D.

Lee, J., Hong, T.K., Park, S., Lee, J., Chung, D., Kim, B., 2022. Laterally varying crustal and quaternary fault-zone structures in the Seoul Metropolitan Area, South Korea, from a joint inversion analysis based on dense seismic arrays. Bull. Seismol. Soc. Am. 112, 1935–1959. https://doi.org/10.1785/0120210197.

Lee, K.S., Chang, H.W., Park, K.H., 1998. Neoproterozoic bimodal volcanism in the central Ogcheon belt, Korea: Age and tectonic implication. Precambr. Res. 89, 47–57. https://doi.org/10.1016/s0301-9268(97)00077-6.

Lee, S.-H., 2016. Study on the upper mantle discontinuities around the Korean Peninsula using teleseismic receiver functions with a CCP stacking method. Seoul National University.

Lee, S.R., Cho, M., Hwang, J.H., Lee, B.J., Kima, Y.B., Kim, J.C., 2003. Crustal evolution of the Gyeonggi massif, South Korea: Nd isotopic evidence and implications for continental growths of East Asia. Precambr. Res. 121, 25–34. https://doi.org/10.1016/S0301-9268(02)00196-1.

Lee, Y.S., Han, H.C., Hwang, J.H., Kee, W.S., Kim, B.C., 2011. Evidence for significant clockwise rotations of the Korean Peninsula during cretaceous. Gondw. Res. 20, 904–918. https://doi.org/10.1016/j.gr.2011.05.002.

Li, Z.-X., 1994. Collision between the north and south China blocks: a crustal-detachment model for suturing in the region east of the Tanlu Fault. Geology 22, 739–742. https://doi.org/10.1130/0091-7613(1994)022<0739:CBTNAS>2.3.CO;2.

Long, M.D., Silver, P.G., 2009. Mantle flow in subduction systems: the subslab flow field and implications for mantle dynamics. J. Geophys. Res. 114, B10312. https://doi.org/10.1029/2008JB006200.

Long, M.D., van der Hilst, R.D., 2005. Upper mantle anisotropy beneath Japan from shear wave splitting. Phys. Earth Planet. In. 151, 206–222. https://doi.org/10.1016/j.pepi.2005.03.003.

Ma, J., Bunge, H.P., Fichtner, A., Chang, S.J., Tian, Y., 2023. Structure and Dynamics of Lithosphere and Asthenosphere in Asia: a Seismological Perspective. Geophys. Res. Lett. 50. https://doi.org/10.1029/2022GL101704.

Mainprice, D., Silver, P.G., 1993. Interpretation of SKS-waves using samples from the subcontinental lithosphere. Phys. Earth Planet. In. 78, 257–280. https://doi.org/10.1016/0031-9201(93)90160-B.

Niu, Y., Tang, J., 2016. Origin of the Yellow Sea: an insight. Sci. Bull. 61, 1076–1080. https://doi.org/10.1007/s11434-016-1113-z.

Oh, C.W., 2006. A new concept on tectonic correlation between Korea, China and Japan: Histories from the late Proterozoic to cretaceous. Gondw. Res. 9, 47–61. https://doi.org/10.1016/j.gr.2005.06.001.

Oh, C.W., Choi, S.G., Song, S.H., Kim, S.W., 2004a. Metamorphic evolution of the baekdong metabasite in the Hongseong area, South Korea and its relationship with the Sulu collision belt of China. Gondw. Res. 7, 809–816. https://doi.org/10.1016/s1342-937x(05)71065-0.

Oh, C.W., Imayama, T., Jeon, J., Yi, K., 2017. Regional Middle Paleozoic metamorphism in the southwestern Gyeonggi Massif, South Korea: its implications for tectonics in Northeast Asia. J. Asian Earth Sci. 145, 542–564. https://doi.org/10.1016/j.jseaes.2017.06.030.

Oh, C.W., Kim, S.W., Choi, S.G., Zhai, M., Guo, J., Krishnan, S., 2005. First finding of eclogite facies metamorphic event in South Korea and its correlation with the Dabie-Sulu collision belt in China. J. Geol. 113, 226–232. https://doi.org/10.1086/427671.

Oh, C.W., Kim, S.W., Ryu, I.C., Okada, T., Hyodo, H., Itaya, T., 2004b. Tectono-metamorphic evolution of the Okcheon Metamorphic Belt, South Korea: Tectonic implications in East Asia. Isl. Arc 13, 387–402. https://doi.org/10.1111/j.1440-1738.2004.00433.x.

Otofuji, Y., ichiro, Kambara, A., Matsuda, T., Nohda, S., 1994. Counterclockwise rotation of Northeast Japan: Paleomagnetic evidence for regional extent and timing of rotation. Earth Planet. Sci. Lett. 121, 503–518. https://doi.org/10.1016/0012-821X(94)90087-6.

Otofuji, Y.I., Matsuda, T., 1987. Amount of clockwise rotation of Southwest Japan - fan shape opening of the southwestern part of the Japan Sea. Earth Planet. Sci. Lett. 85, 289–301. https://doi.org/10.1016/0012-821X(87)90039-2.
Otofuji, Y.I., Matsuda, T., 1983. Paleomagnetic evidence for the clockwise rotation of Southwest Japan. Earth Planet. Sci. Lett. 62, 349–359.
Otofuji, Y.I., Matsuda, T., Nohda, S., 1985. Opening mode of the Japan Sea inferred from the palaeomagnetism of the Japan Arc. Nature 317, 603–604. https://doi.org/10.1038/317603a0.
Pacanovsky, K.M., Davis, D.M., Richardson, R.M., Coblentz, D.D., 1999. Intraplate stresses and plate-driving forces in the Philippine Sea Plate. J. Geophys. Res. 104, 1095–1110. https://doi.org/10.1029/98jb902845.
Park, S., Hong, T.K., 2024a. Correct off-site determination of seismic sensor orientation from combined analyses of earthquake and microseism records. Bull. Seismol. Soc. Am. 114, 942–954. https://doi.org/10.1785/0120230150.
Park, S., Hong, T.K., 2024b. Continent-side uplifted mantle and geological imprints along a paleo rift in the western east sea (sea of Japan). J. Geophys. Res. Solid Earth 129. https://doi.org/10.1029/2024JB029049.
Park, S., Hong, T.K., Kim, B., Lee, J., 2023. Role of Backbone Fault System on Earthquake Spawning and Geohazards in the Seoul Metropolitan Area. Earth Sp. Sci. 10, 1–24. https://doi.org/10.1029/2022EA002686.
Park, S., Hong, T.K., Rah, G., 2021. Seismic hazard assessment for the korean peninsula. Bull. Seismol. Soc. Am. 111, 2696–2719. https://doi.org/10.1785/0120200261.
Park, S.I., Kim, S.W., Kwon, S., Santosh, M., Ko, K., Kee, W.S., 2017. Nature of late Mesoproterozoic to Early Neoproterozoic magmatism in the western Gyeonggi massif, Korean Peninsula and its tectonic significance. Gondw. Res. 47, 291–307. https://doi.org/10.1016/j.gr.2016.11.006.
Park, S.I., Kwon, S., Kim, S.W., Yi, K., Santosh, M., 2014. Continental origin of the Bibong eclogite, southwestern Gyeonggi massif, South Korea. J. Asian Earth Sci. 95, 192–202. https://doi.org/10.1016/j.jseaes.2014.08.024.
Petrishchevsky, A.M., 2022. Extension and strike-slips in the crust of the yellow sea (probabilistic gravity model). Oceanology 62, 247–257. https://doi.org/10.1134/S0001437022020138.
Plomerová, J., Šílený, J., Babuška, V., 1996. Joint interpretation of upper-mantle anisotropy based on teleseismic P-travel time delays and inversion of shear-wave splitting parameters. Phys. Earth Planet. In. 95, 293–309. https://doi.org/10.1016/0031-9201(95)03122-7.
Ree, J.H., Cho, M., Kwon, S.T., Nakamura, E., 1996. Possible eastward extension of chinese collision belt in South Korea: the Imjingang belt. Geology 24, 1071–1074. https://doi.org/10.1130/0091-7613(1996)024<1071:PEEOCC>2.3.CO;2.
Sajeev, K., Jeong, J., Kwon, S., Kee, W.S., Kim, S.W., Komiya, T., Itaya, T., Jung, H.S., Park, Y., 2010. High P-T granulite relicts from the Imjingang belt, South Korea: tectonic significance. Gondwana Res. 17, 75–86. https://doi.org/10.1016/j.gr.2009.07.001.
Savage, M.K., 1999. Seismic anisotropy and mantle deformation: what have we learned from shear wave splitting? Rev. Geophys. 65–106. https://doi.org/10.1029/98RG02075.
Shih, X.R., Meyer, R.P., Schneider, J.F., 1989. An automated, analytical method to determine shear-wave splitting. Tectonophysics 165, 271–278.
Silver, P.G., 1996. Seismic anisotropy beneath the continents: probing the depths of geology. Annu. Rev. Earth Planet. Sci. 24, 385–432. https://doi.org/10.1146/annurev.earth.24.1.385.
Silver, P.G., Chan, W.W., 1991. Shear wave splitting and subcontinental mantle deformation. J. Geophys. Res. 96, 16429–16454.
Silver, P.G., Chan, W.W., 1988. Implications for continental structure and evolution from seismic anisotropy. Nature 335, 34–39.
Silver, P.G., Savage, M.K., 1994. The interpretation of shear-wave splitting parameters in the presence of two anisotropic layers. Geophys. J. Int. 119, 949–963.
Sohn, Y.K., Park, K.H., 2004. Early-stage volcanism and sedimentation of Jeju Island revealed by the Sagye borehole, SW Jeju Island, Korea. Geosci. J. 8, 73–84. https://doi.org/10.1007/bf02910280.
Son, M., Song, C.W., Kim, M.C., Cheon, Y., Cho, H., Sohn, Y.K., 2015. Miocene tectonic evolution of the basins and fault systems, SE Korea: Dextral, simple shear during the East Sea (Sea of Japan) opening. J. Geol. Soc. London 172, 664–680. https://doi.org/10.1144/jgs2014-079.
Song, J.-H., Kim, S., Rhie, J., 2020. Heterogeneous modification and reactivation of a craton margin beneath the Korean Peninsula from teleseismic travel time tomography. Gondw. Res. 81, 475–489. https://doi.org/10.1016/j.gr.2019.11.016.
Song, J.H., Kim, S., Rhie, J., Lee, S.H., Kim, Y.H., Kang, T.S., 2018. Imaging of lithospheric structure beneath Jeju Volcanic Island by teleseismic traveltime tomography. J. Geophys. Res. Solid Earth 123, 6784–6801. https://doi.org/10.1029/2018JB015979.
Uno, K., 2000. Clockwise rotation of the Korean Peninsula with respect to the North China Block inferred from an improved Early Triassic palaeomagnetic pole for the Ryeongnam Block. Geophys. J. Int. 143, 969–976. https://doi.org/10.1046/j.0956-540X.2000.01289.x.
Vaes, B., van Hinsbergen, D.J.J., Boschman, L.M., 2019. Reconstruction of subduction and back-arc spreading in the NW Pacific and aleutian basin: clues to causes of cretaceous and eocene plate reorganizations. Tectonics 38, 1367–1413. https://doi.org/10.1029/2018TC005164.
Vinnik, L., Romanowicz, B., Le Stunff, Y., Makeyeva, L., 1995. Seismic anisotropy in the D“ layer. Geophys. Res. Lett. 22, 1657–1660.
Wolfe, C.J., Silver, P.G., 1998. Seismic anisotropy of oceanic upper mantle: Shear wave splitting methodologies and observations. J. Geophys. Res. Solid Earth 103, 749–771. https://doi.org/10.1029/97jb02023.
Wüstefeld, A., Bokelmann, G., 2007. Null detection in shear-wave splitting measurements. Bull. Seismol. Soc. Am. 97, 1204–1211. https://doi.org/10.1785/0120060190.
Yang, G., Zhao, L.F., Xie, X.B., He, X., Yan, L., Yao, Z.X., 2022. “Double door” opening of the Japan Sea Inferred by Pn attenuation tomography. Geophys. Res. Lett. 49, 1–10. https://doi.org/10.1029/2022GL099886.
Yin, A., Nie, S., 1993. An indentation model for the north and south China collision and the development of the Tan-Lu and honam fault systems, Eastern Asia. Tectonics 12, 801–813.
Zhai, M., Guo, J., Li, Z., Chen, D., Peng, P., Li, T., Hou, Q., Fan, Q., 2007. Linking the Sulu UHP belt to the Korean Peninsula: evidence from eclogite, Precambrian basement, and Paleozoic sedimentary basins. Gondw. Res. 12, 388–403. https://doi.org/10.1016/j.gr.2007.02.003.
Zhang, K.J., 1997. North and South China collision along the eastern and southern North China margins. Tectonophysics 270, 145–156. https://doi.org/10.1016/S0040-1951(96)00208-9.
Zhang, S., Karato, S., 1995. Lattice preferred orientation of olivine aggregates in simple shear. Nature 375, 774–777.
Zhao, T., Zhu, G., Lin, S., Wang, H., 2016. Indentation-induced tearing of a subducting continent: evidence from the Tan-Lu Fault ZonC, East China. Earth-Sci. Rev. 152, 14–36. https://doi.org/10.1016/j.earscirev.2015.11.003.